Visualization toolkit for image quality assessment in digital radiography

Master Thesis

For attainment of the academic degree of
Master of Science in Engineering (MSc)

in the Master Program Digital Healthcare
at St. Pölten University of Applied Sciences

by
Christian Schneckenleitner, MSc
dh151832

First advisor: Prof.FH Dipl. Ing. Matthias Husinsky
Second advisor: Mag. Alexander Rind

St.Pölten, 17.08.2017

Declaration

I declare that I have developed and written the enclosed Master Thesis completely by myself, and have not used sources or means without declaration in the text. Any thoughts from others or literal quotations are clearly marked. This work was not used in the same or in a similar version to achieve an academic grading or is being published elsewhere.

Amstetten, 17.8.2017

Place, Date Signature

Abstract

A routinely performed radiograph is taken by radiographers in their daily routine. For example, a typical wrist or ankle examination consists of two or more images taken with standardized acquisition parameters. These parameters are generic adoptions and should be optimized on the basis of the detector system and the X-ray components. The particular acquisition parameters for each radiograph depend on the radiographer's experience and background knowledge. There is no noticeable support system and technology to provide ideal parameters for high-quality images in digital radiography.

However, technologies for data analysis and visualization constitute a considerable body of research in other fields of work. Thus, particular solutions are related to specific user groups and working environments. Within this scope, a dashboard for local contrast assessment in digital radiography is introduced. The leading question in this context is: "Which graphic data representation influences the informed choice for image optimization?" To explore, a proof of concept is executed to determine the usefulness of the visualization of image quality within a dashboard for modern radiography. A dashboard is established to outline the visualization of local contrast behaviors over a full range of acquisition parameters for radiographs.

The entire academic work is divided into image acquisition, image processing and metric calculation, dashboard development, and dashboard evaluation and analysis. The related theoretical topics are X-rayed physics, radiological imaging, image processing, and data visualization.

All radiographs were taken under laboratory conditions. The main result of this thesis is a dashboard for image quality assessment for radiographers. The dashboard assessment by an expert determination, evaluation, and model-based analysis was done. The used Weber contrast metric is valid for image quality assessment. The expert statements pointed out an added value for radiographers in their daily work base.

Kurzfassung

Röntgenaufnahmen werden von Radiologietechnologen und Radiologietechnologinnen in ihrer täglichen Arbeit angefertigt. Eine typische Handgelenk- oder Knöcheluntersuchung besteht aus zwei oder mehr Bildern, welche mit standardisierten Aufnahmeparametern aufgenommen werden. Diese Parameter sind allgemeine Annahmen und müssen an das Detektorsystem, die Gerätekomponenten und die Eigenschaften des Organbereichs angepasst werden. Die Wahl der Aufnahmeparameter für jedes Röntgenbild sind abhängig von der Erfahrung der Radiologietechnologen und Radiologietechnologinnen und deren fachlichen Hintergrundwissen. Um qualitativ hochwertige Bilder in der digitalen Radiographie zu generieren, stehen keine Experten und Expertinnensysteme oder unterstützende Technologien im klinischen Alltag zur Verfügung. Allerdings sind derartige technologische Lösungen für Datenanalysen und Visualisierungen ein zentrales Thema in anderen Arbeitsbereichen.

Im Rahmen der Arbeit wird ein Dashboard zur lokalen Kontrastbewertung in der digitalen Röntgenaufnahmen entwickelt. Die Leitfrage in diesem Kontext lautet: "Welche grafische Datenrepräsentation beeinflusst die Wahl für die Bildoptimierung?" Um diese Frage valide zu beantworten, wird ein Dashboard entwickelt, um die Machbarkeit einer Bildqualitätsvisualisierung für die moderne Radiographie zu bewerten. Hierfür wird ein Prototyp verwendet, mit welchem das lokale Kontrastverhalten über den gesamten Aufnahmebereich für Röntgenaufnahmen visualisiert wird.

Die wissenschaftliche Arbeit ist in Bildakquisition, Bildverarbeitung und Berechnung der Kontraste, Dashboard-Entwicklung und die Auswertung und Analyse gegliedert. Die verwandten theoretischen Themen sind Strahlenphysik, radiologische Bildgebung, Bildverarbeitung und Datenvisualisierung.

Das Hauptergebnis dieser Arbeit ist ein Dashboard zur Bildqualitätsbewertung für Radiologietechnologen und Radiologietechnologinnen. Die Dashboard-Bewertung wurde von Experten durchgeführt und eine Evaluation und modellbasierte Analyse wurde durchgeführt. Der verwendete Weber-Kontrast und eine Falschfarben Darstellung gilt für die Bildqualitätsbewertung als valide. Die Expertenbewertung zeigte einen Mehrwert für Radiologietechnologen und Radiologietechnologinnen im täglichen Arbeitsalltag.

Table of Contents

1 Introduction

"You cannot step twice into the same river". Heraclitus (c. 535 B.C.)

There is a deeper meaning of images, especially radiological images, behind this philosophical utterance. In Heraclitus' statement, the identity of an object is formed by the riverbed and shaped by clear lines. These are phenotypical aspects of the river. On the contrary, water represents the dynamic property of the scenery. Water flows do not influence the higher being of the phenotype and gives the river a unique moment. During data acquisition, the discrete detector elements, the range of numbers per pixel, i.e. the bit depth, and the matrix size represents the steady riverbed. During X-ray exposure, the nature of photons and the image acquisition process itself underlie statistical and electronic effects and cannot be taken twice in the same manner. From this vantage point, we can find this dualism between a well-formed object and the phenotypical aspects as part of the radiological acquisition process.

In planar radiography, general recommendations for the selection of suitable exposition parameters exist in the basic literature—for example, a wrist radiograph is taken with 60kV and 1.3mAs [1]. To go into detail, an ideal parameterization depends on the properties of the transmitted object, the used X-ray detector system, and the geometrical set-up. Radiographers are, however, not equipped with adequate tools to achieve the best possible organ optimization and individual parameter adaptation at their daily work base.

An expert system for visualizing the image quality of gray-value intensity distributions in radiographs could be suitable feedback for radiographers. For this purpose, the most important exposition parameters are considered and local contrasts are obtained from the image raw data. The kilovolt (kV) and the milliampere-second product (mAs) are the most imported acquisition parameters while taking radiographs; they influence the image appearance and subsequently the medical reports. An image quality dashboard based on kV and mAs and their influence on local contrast behavior within radiographs could provide an adequate solution for radiographers.

1 Introduction

The objective of this thesis was to find the capability of visualizing the local contrast behaviors for various acquisition parameters within a radiograph. The aim was to develop a dashboard to picture the needed information to determine the local contrast in one single page. The main focus was on establishing and visualizing numerical image contrast as false color tables. The main interest in this scientific work was to visualize the impact of local contrast behavior based on the acquisition parameters kV and mAs.

A scientific setup was planned and structured into different work packages. The empirical process was divided into four main sections.

The first work package included the definition of the test set for the X-ray acquisition process. In this regard, the test phantom, the experimental setting, and the acquisition parameters were well chosen.

In the second step, the contrast features within the radiographs, extraction of the required metrics, and calculation of the local contrasts were defined. Following this, false color tables and the needed additional visualization elements were created and a full image quality dashboard was developed.

The image quality dashboard was introduced to medical image experts to determine the dashboard for image quality assessment. In this approach, open questions were formed. Finally, the image quality metric was evaluated and a model-based dashboard analysis was executed.

2 Theoretical Background for Image Quality Visualization

The following chapter contains the theoretical background of physical principles and digital imaging systems for plain radiography, image processing, and analyses in radiology, data visualization, and determination methods for user acceptance. In its present form, the subchapters cover the required theoretical background to describe the needed topics and raise no claim to completeness.

The subchapter order is based on the chronological work task for the requirement, implementation, and testing phase of this thesis.

2.1 Digital imaging systems

Plane radiological images are produced by different X-ray modalities like mammography, angiography, fluoroscopy, or skeletal units. These imaging modalities are used for specific clinical applications in different environments of radiology departments, operation theaters, or interventional rooms. Most devices use ionizing radiation—the so-called X-rays—to generate digital intensity images. There are different techniques and clinical procedures as well as examinations to gather data from digital X-ray units, depending on the used modality and needed medical information.

Furthermore, digital X-ray imaging units are part of the picture archiving and communication system (PACS). Dreyer et al. [2] have listed image acquisition, PACS core, and interpretation workstations as basic elements within a digital radiology department. An extended model by Wang et al. [3] describes advanced image visualization tools to process and analyze radiological images and datasets for clinical assessments.

In a narrower sense, the X-ray imaging system consists of different components [4]. The X-rays are generated by the X-ray tube unit and the high voltage generator. The detector system collects the object-permeated signal and converts the analog signal into the digital domain. [5]

Taken as a whole, the linear system theory describes the output g as a function of the input f. The transfer function H is the responsive function of an imaging system. A projective radiological imaging system can be described as [6]:

$$g(x,) = H\{f(x,y)\}$$

For example, in Figure 1, a skull phantom is the input g, while the X-ray represents the output from the imaging system.

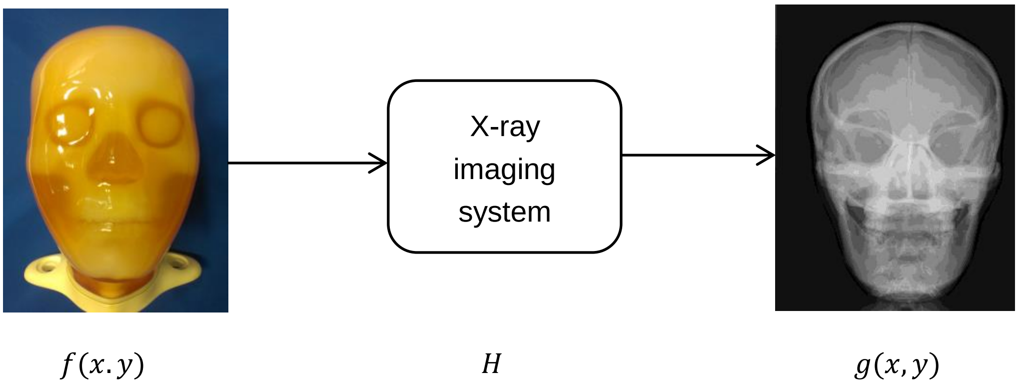

Figure 1. Linear system theory and X-ray imaging

From a more complex point of view, the operating mode and acquisition parameters of the X-ray unit influence the nature of the photons on the detector system. Inside the detector system, the analog signal is converted into a digital matrix. The result is a raw X-ray image that represents the density distribution of the object. The representation of the generated image is optimized for the structure of interest. This processed radiograph is the final result of a diagnostic examination. A generic workflow overview has been pictured in Figure 2.

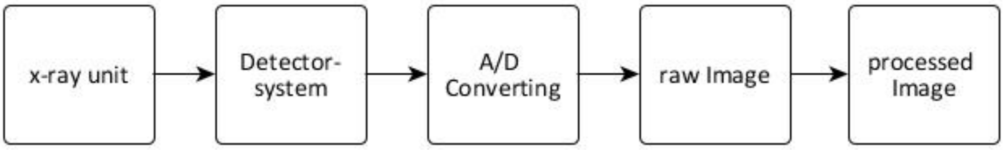

Figure 2. Generic overview of an imaging process

Medical imaging devices use a broad spectrum of ionizing radiation to deliver information from differentiable structures to generate characteristic image sensations. According to that, different body part examination requires variable physical exposure parameters for each imaging process [6], [7]. The relation between differentiable body parts and the physical exposure parameter is uncertain and part of scientific work.

A well-known and practically applied method is the "As Low As Reasonably Achievable" (ALARA) principle. The first part "as low as reasonable" refers to the applied patient dose and the second part is "achievable" to meet the desperately needed diagnostic requirements [8].

2.1.1 Basic principles of physics in radiography

An X-ray tube and detector system are essential components of the imaging device. X-rays are generated when electrons interact with materials. First, the electrons are accelerated by high voltage from the cathode to the anode, which is a metallic material. As much as 99% of the kinetic energy is emitted as heat and 1% is transformed into electromagnetic energy, namely X-rays [9]. The higher the kinetic energy of the electrons with the generation of more X-ray photons, the higher is their energy. During this process, a typical X-ray spectrum is shaped. Figure 3 pictures a filtered schematic X-ray spectrum of diagnostic imaging devices. By definition, the wavelength of X-ray is within the range of electromagnetic waves. Krieger [10] has denoted the wavelength of X-ray radiation between $3 * 10^{-8} m$ and $6 * 10^{-17} m$.

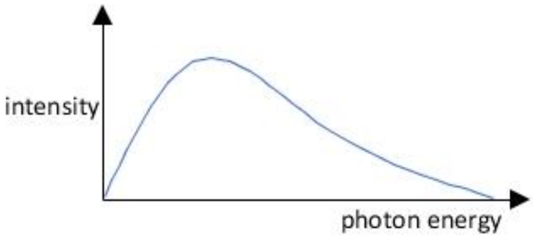

Figure 3 Schematic shape of an X-ray spectrum

The electromagnetic interaction of these photons or X-rays with material underlies the physical principle of the Beer–Lambert law [9]. It implies exponential decay of the intensity by increasing the material thickness. The exponential attenuation law is valid for a narrow parallel mono-energetic radiation beam and describes the decreasing primary quants. The transmission T_x denotes the primary X-ray quants T_x behind an absorber x and the primary X-ray quants before the absorber:

$$T_x = \frac{N_x}{N}$$

The exponential expression of the attenuation law under certain requirements are formulated with the scope of the intensity for a given thickness of I_d:

$$I_d = I_0 * e^{-\mu * d}$$

The intensity I_0 represents the primary X-ray quants intensity and the exponential part on the right confirms the transmission T.

Figure 4 points out the intensity distribution behind an object. The line–plot symbolizes the principle of X-ray images and the attenuation of X-rays.

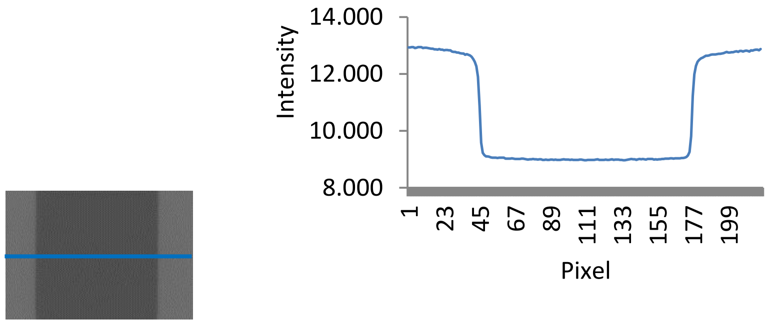

Figure 4. Intensity distribution of X-ray behind simple objects

The blue line on the left image pictures on the drawn line in the profile plot. On the right of Figure 4, the corresponding gray value function is plotted along a pixel line.

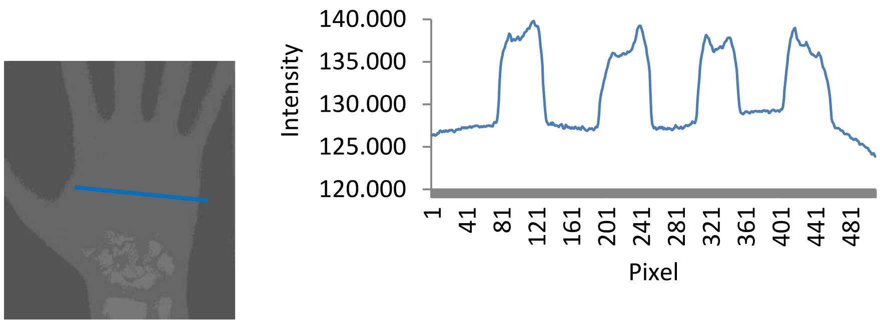

Figure 5. Intensity distributions of wrist bones and soft tissues

Figure 5 points out a more sophisticated situation. The soft tissue and bone structures are in a projective superposition, and the gray scale intensity represents the attenuated sum of the two structures. The intensity distribution of the wrist is pictured as a radiograph. The representation is done as an inverted image from the measured detector signal. Behind the bone structure, less signal is measured on the detector system and the gray value is presented in a brighter shade of gray. In contrast, the anatomical structure is pictured in a darker shade of gray or black against the background. As shown in Figure 5, more absorption in the tissue refers to less signal on the detector system and a brighter gray value in the radiograph.

There are three forms of interaction for ionizing photons with the material. In diagnostic radiography, two main processes are prevalent, namely the photo effect and the Compton effect. [10]

By elastic collision, a photon releases an electron from an inner shell within the atomic nucleus. This process is called the photo effect and one of the dominant forms of interaction with the material in diagnostic imaging. This energy-depended effect of the photon absorption τ can be expressed as: [10]

$$\tau \propto \rho * \frac{Z^{n+1}}{A * E_\gamma^3} \approx \rho * \frac{Z^n}{E_\gamma^3}$$

Delineated from the expression, the photon energy and the photon absorption are inversely proportional. By increasing the tube potential, the photon energy increases and the photo effect probability decreases. Conversely, the atomic number Z is proportional, which means that the higher the atomic number, the higher the probability for the photo effect.

The inelastic correlation between a photon and the outside electrons is called the Compton effect. The photon momentum is partly conveyed to an electron and the photon distracted from the primary direction – in other words, scattered. The probability for this effect can be expressed as the Compton-interaction-coefficient σ_c.

$$\sigma_c = \propto \rho * \frac{Z}{A} * \frac{1}{E_\gamma^n} \neq f(Z)$$

The Compton effect depends less on the photon energy and is the dominant effect in higher ranges. Similar to the photo effect, the Compton effect is proportional to the atomic number.

The laws of atom physics influence the appearance of radiographs and the image quality in an essential way.

2.1.2 Origins of contrast in the X-ray image

There are different contrast types and definitions in digital detector systems. Image contrast can generally be defined as the signal difference between the average signals. In X-ray imaging, the contrast depends on the attenuation of the subject and the background. The higher the image contrast, the more features can be distinguished by professionals. This characteristic is mainly influenced by the produced X-ray spectrum. In addition to laws of atom physics, the contrast between radiographic images is affected by the detector system and the conversion process.

There are two different types of contrast in radiographic images: The Weber contrast is for local measurements and the modulation contrast to perform Fourier analysis is seen in medical imaging. The Weber contrast C_w is defined as:

$$C_w = \frac{f_f - f_b}{f_b}$$

The signal of the feature f_b against the background f_b represents the local contrast.

2.1.3 Fundamentals of acquisition parameters

Image quality is mainly influenced by the chosen acquisition parameters. The image characteristic is defined by the operation mode of the X-ray tube and the type of hardware components used to take the radiograph. The images in Figures 6, 7, 8 were taken with 48kV, 77kV, and 109kV respectively along with fixed 20 milli ampere seconds (mAs). This comparison depicts three different tube currents and displays their different intensity distributions.

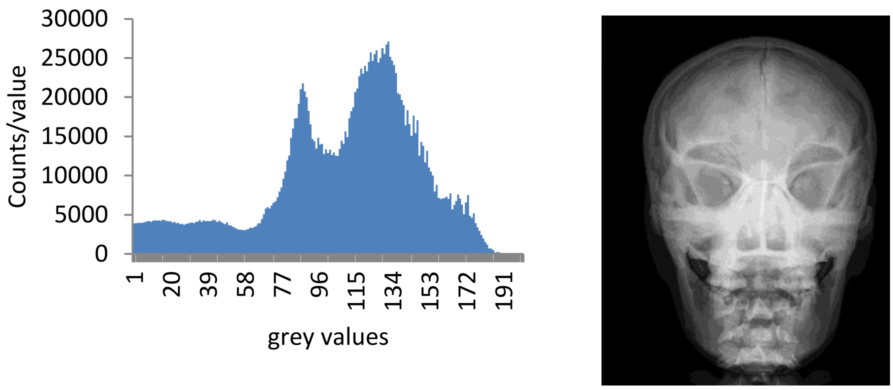

Figure 6. The histogram and X-ray of a skull phantom taken with 48kV

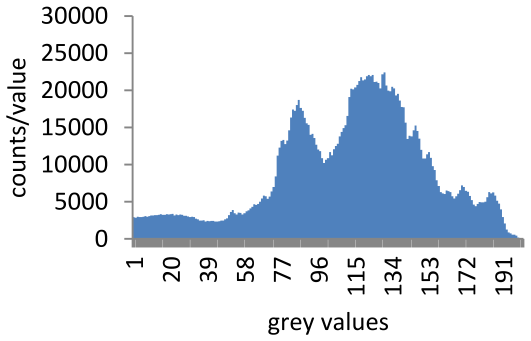

Figure 7. The histogram and X-ray of a skull phantom taken with 77kV

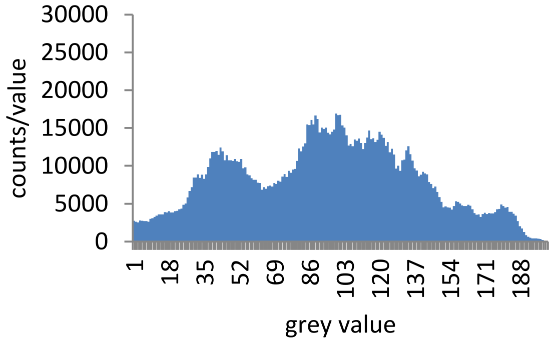

Figure 8. The histogram and X-ray of a skull phantom taken with 109kV

The gray scale shift in the histogram is well-founded in a decreased signal on the detector. Uffmann et al. have approved different study protocols to determine image quality [11]. They have selected different tube voltages to perform chest X-rays and measured a significantly different visibility of anatomical structures into the radiographs. Similar results on different tube voltages and low contrast detectability have been published by Kun Tagn et al. [12].

2.1.4 Detector technologies for plain radiography

The described X-ray detector technologies raise no claim to completeness. The named types are the commonly available systems in plane radiography for different clinical applications.

In 1983, Sonoda et al. [13] published and introduced the first digital imaging technology for projection modalities by Fuji (Tokyo, Japan). This key-turn technology was the beginning of digital imaging systems and data processing in radiology. Since then, advances in new imaging processing have driven modern healthcare systems in radiology.

In 2002, Kotter et al. [14] introduced a classification and listed different digital X-ray systems for plain radiography:

- Portable systems
- Storage phosphor radiography
- Conventional storage phosphor plates
- Needle–crystalline screens
- Stationary systems
- The selenium detector with an electrometer readout (Thoravision system)
- Scintillators with CCD camera
- Flat-panel detectors (with TFT panels)
- Indirect conversion of X-rays (scintillators with photodiode and
- TFT readout)
- With non-structured scintillator
- With structured (needle-shaped) scintillator
- Direct conversion of X-rays
- Photoconductor+TFT-panel readout

This comprehensive overview can be simplified and distracted into two main domains, namely the computed radiography systems (CR) and digital radiography detectors systems (DR). Considering this, Lanca et al. [5] have illustrated different technologies in a schematic chart.

The CR technology uses a storage phosphor plate to capture energy from X-rays. The acquisition process is similar to the conventional analog imaging workflow. The acquisition parameters (kV, mAs), the X-ray tube, the examination table, and conventional cassette sizes are the same. The main difference between analog and computed radiography systems is the X-ray-capturing process by the phosphor plate. CR technology generates some kind of latent energy distribution on the detector plate [15]. The local varying energy levels on the phosphor plate are equal to a number of converted X-rays. A laser beam measures the emitted light signal of trapped energy in the phosphor plate and does the read-out process. The stored energy is set free as visible light and an analogue–digital converter generates a corresponding digital image matrix. The whole process is performed by a read-out device, as shown in Figure 10. The image matrix is sent to an image-processing workstation to assess the quality of the taken image. The image-processing workflow is shown in Figure 9.

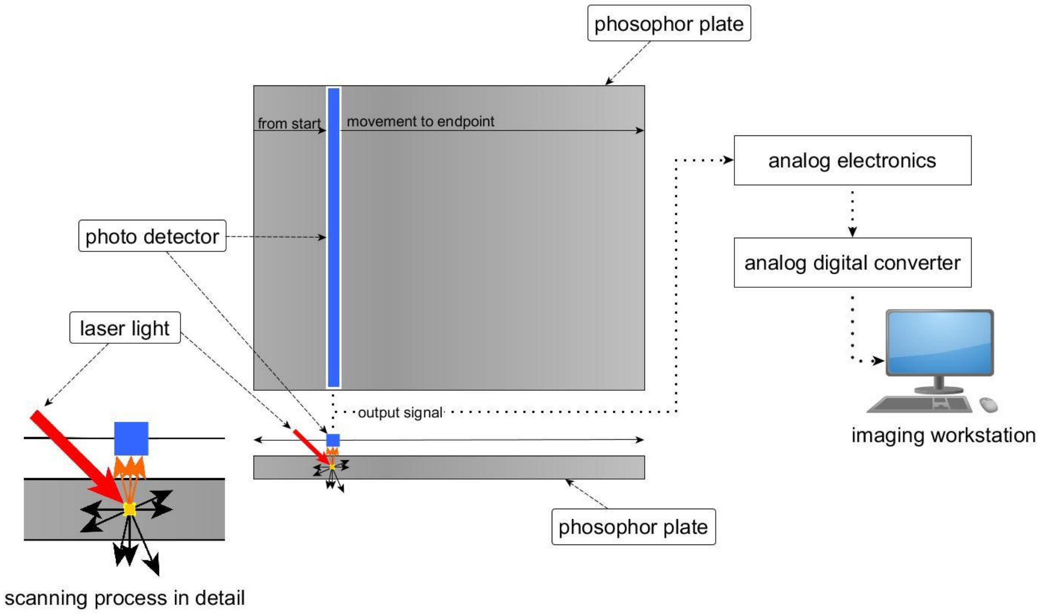

Figure 9. Computed radiography (CR) scanning process

Figure 10 gives an overview of the technology component, which is used to take a CR image.

Image cassette phosphor plate read out device image workstation

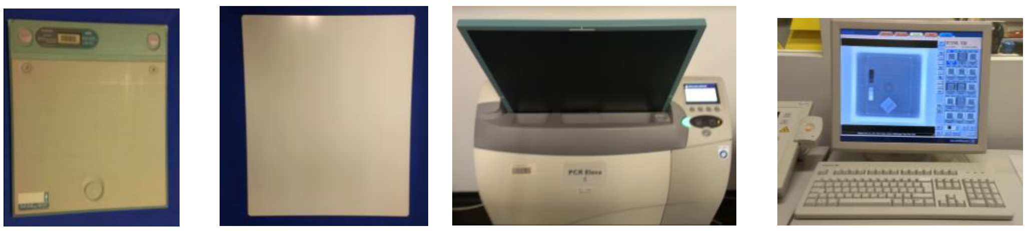

Figure 10. Computed radiography imaging components

DR imaging systems are realized with large area flat panel detectors. Typically, detective area sizes are 35x43cm or 24x30cm. By definition, a flat panel detector system is described as the following:

> *A radiographic flat-panel detector is a digital, electronically readable radiography system. By definition, the detector is a slim system (flat panel) that can be integrated into existing Bucky tables.* [14]

Such flat panel detector systems can categorically be divided into two main branches based on different energy transformation methods. Both systems are described by their imaging and conversation processes.

The indirect technology is pictured in Figure 11 and illustrates the components. From top to bottom, the conversion process can be read. The wavelength of X-ray photons is converted within the scintillator layer and then transferred into visible light. The amount of the produced visible light is turned into electrical charge and the readout process is performed by the underlying TFT matrix.

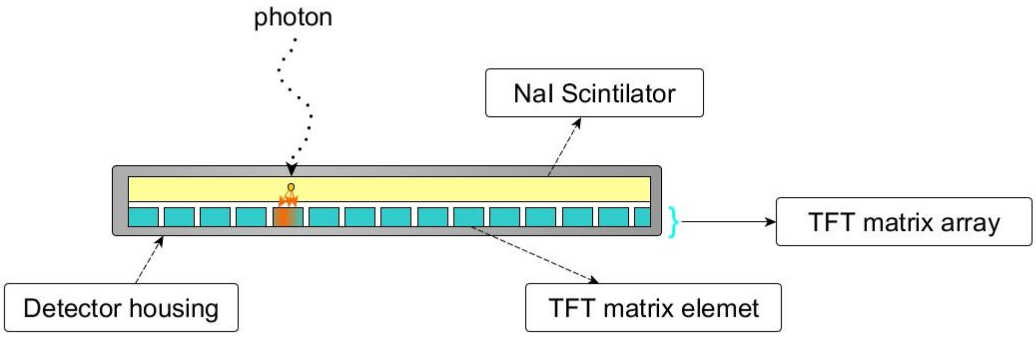

Figure 11. Digital radiography (DR) scanning process for indirect flat panel detector systems

The nature and material of the scintillator material is a main factor of capturing photons and producing high-quality radiographs. In most diagnostic systems, the scintillator is a cesium iodine crystal, and in this case, lateral light diffusion influences the spatial resolution. To minimize this problem, scintillator crystals are grown from the TFT-matrix plane to the photon-sided surface. The use of structured needle crystals allows a thicker scintillator layer under equal spatial resolution and higher detective quantum efficiency of the detector system. [14]

A direct X-ray detector converts photons without producing any visible light into electric charges by using a photoconductor layer. The direct connection between the photoconductor layer and the TFT matrix allows higher spatial resolution compared with indirect systems. X-ray exposition on the photoconductor composed of amorphous selenium generates electrons and holes within the material. Because of the electric field, the produced charges are migrated and the charge-collector collection is stored. An affiliated electronic does the readout and digitization process.

Independent of the used technology—either a CR or a DR system, or an indirect or direct conversion process—the intention to use the digital system existing in modern radiology departments. Williams et al. [16] have identified the motivation to use digital systems. This leads to the following central statements:

1) In comparison with the analog image acquisition, a larger range of beam intensity can be imaged on a digital detector system
2) The wide independence of the contrast representation from the tube voltage used (kVp) by the adjustment of the window width at the receiving console
3) The independence of image brightness from the selected milliampere seconds by the adjustment of the window level
4) The availability of image-processing stations and evaluation programs to improve the analysis
5) For easier and more reliable identification and labeling of image data
6) The possibility of digital transmission, storage, and presentation for interpretation, diagnosis, and consolidation of images

Two among the six core statements refer to the acquisition parameters kV and mAs and their influence on X-ray images. One assertion leads to the evaluation programs to improve the analysis.

Furthermore, Williams et al. have provided the key elements to perform high-quality digital radiology [16]:

1) The development of secure acquisition protocols to ensure image quality and radiation dose independent of the examination room and the used workstation station
2) Use of adequate image compression to ensure data transfer and storage as well as no loss of clinical information
3) The archiving methods for medical data to make it possible to request the information in a timely manner
4) The possibility of image processing to represent a higher quality of the acquired information
5) Maintain the required state and federal regulations
6) Maintaining confidentiality
7) Minimizing the occurrence of poor X-ray image quality
8) Minimization of inappropriate radiation doses against the patient and the professions
9) The establishment of clinical quality development

The contextual relationship between the obtained key elements is explored to get higher image quality, and the local contrast behavior is presented in Statements 1, 3, 4, and 7.

2.1.5 Assessment of image quality

Image quality assessment refers to objectifying the useful content of a diagnostic image to resolve a specific diagnostic task. Barret et al. [17] have described four criteria which an adequate image should accomplish.

The Task: Refers to a well-defined clinical task. Diagnostic imaging is searching and distinguishing anatomical pathologies in healthy structures. In a more technical term, diagnosing means the detection of an object in a homogeneous background. These objects can be micro-calcification, nodules, or deformations in the form of different shapes and intensities.

Image and object properties: The knowledge of the physical and statistical processes of the medical imaging device is important to understand the information within the acquired image. Radiographs are superimposed intensity-projection on a plane detector [18]. The object property of the human anatomy relies on that background and appears in a characteristic way.

Observer: Observations are needed and can either be derived by humans or determined on the basis of models. The model observer method is used to figure out how the image quality would depend on physical and technological image parameters. In a more clinical setting, the human is the decision maker to define the appropriate image quality.

The figure of merit: A figure of merit is the metric that indicates if the image quality fits the intended task. Commonly used merits are the signal-to-noise ratio (SNR), the modulation transfer function (MTF), the contrast-to-noise ratio (CNR), or the noise power spectrum (NPS) . These metrics allow quantification of physical properties in radiological images. Furthermore, some figures of merit are observer-based and represent the accumulated quality captured by the human observer as a receiver operating characteristic curve (ROC).

2.1.6 Physical image quality of digital radiographs

The evaluation of physical parameters based on input and output characteristics for imaging devices can be done with the aid of a “black box” assumption [19]. These parameters can be useful to compare the dynamic range, spatial resolution, and DQE over different systems and their performance.

2.2 Digital imaging processing and analysis

2.2.1 Digital images in radiology

Digital imaging and communication in medicine (DICOM) is the commonly used file format and communication standard in digital radiology commissioned by the American College of Radiology (ACR). This open standard is developed by the National Electrical Manufacturers Association (NEMA). Already with the development of the first computer tomographic systems in 1970, the first digital pictures in the medicine were generated. At that time, the proprietary standards of medical device providers were used. In 1980, the open DICOM standard was published. The DICOM standard, which was founded in 1983, was used to create independent data transmission and image representation for radiological images and data. The current version is the NEMA Standard PS3. The standard addresses the exchange of digital information among different modalities within a radiology department. The ACR–NEMA has written a standard framework with 18 parts. These pages contain all information relevant to the file and the communication standard [20]

DICOM enables the regulated exchange of information among systems and modalities. To preserve the semantic integrity, an object-oriented modeling principle is used. The goal of this object-oriented model is a precise picture of the real-world situation in digital systems. Environments are described by entities and relationships. Thus, we find objects such as a patient, modality, examination in the data model of DICOM from the real world.

For example, the "patient" and "examination" can be seen from a hierarchy and a chronological point of view. The structure of DICOM follows the investigation logic. The patient is at the top. This can be one of several investigations. An investigation is again composed of the series produced. The individual series consists of the elementary pictures that were acquired. The information content of an entity is determined by attributes—for example, the patient entity is identified by the patient name, ID, sex, and date of birth. These are added to external systems (radiology information system, hospital information system) or by hand (annotations). Looking at the model from a chronological perspective, the following clinical procedure can be described: In the first instance, patient data is collected and called up by a corresponding specialist at a specific modality (CT, PET, US). The devices are used to generate images, image sequences, video recordings, or bio-signals. Depending on the assignments, the corresponding recordings are made and stored in an image archiving and communication system (PACS) in an image data archive. Next, the series or digital data can be collected on a later date with the same patent data record. Figure 12 pictures the relationship and hierarchical structure in DICOM.

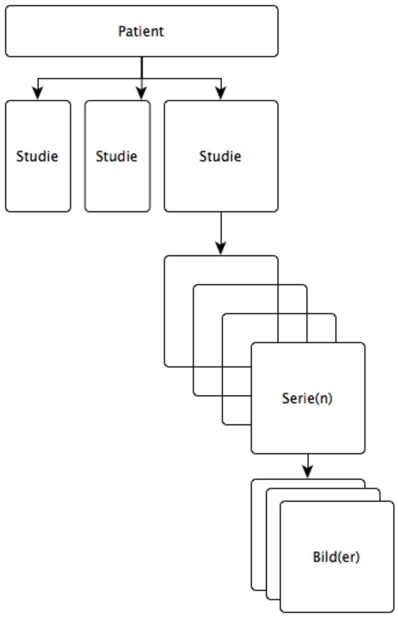

Figure 12. DICOM file structure in radiology

Unique identifiers (UID) have a special meaning for the data header. These are responsible for the clear assignment of a study, series and the instances (images). Using these data, images can be logically assigned and structured to an examination. Each patient, study, series, and image have a unique identification number indicating the affiliation and location of the data objects. Furthermore, the identification number and attributes are used for a structured file search on the studies, series or images level in an image database. Thus, the search filters can be set according to specific studies of the last two years. Figure 13 illustrates the schematic model of a data set based on UIDs. [21]

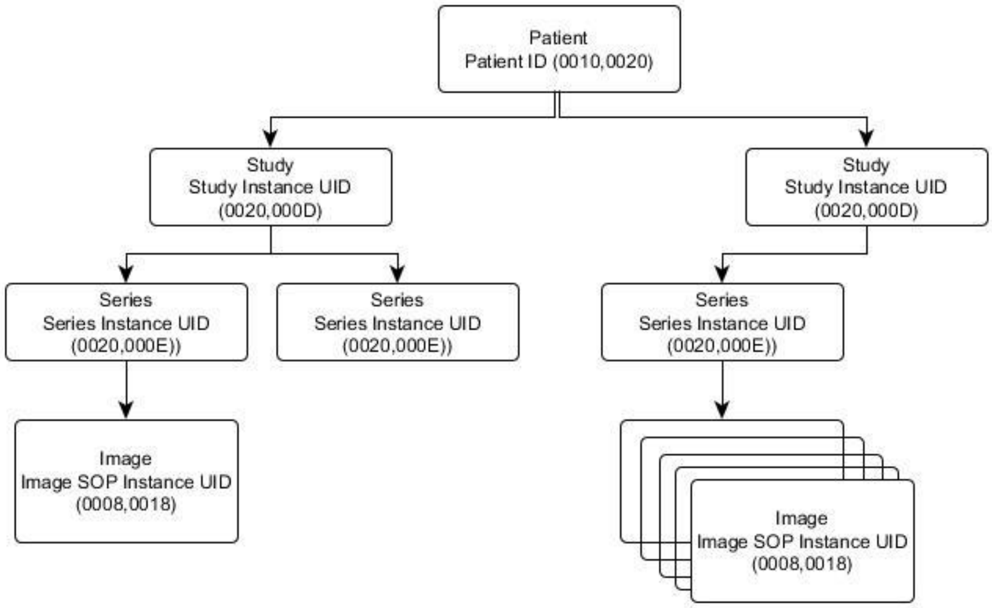

Figure 13 Unified identifier in a generic DICOM structure

Data elements in DICOM are the elementary information held within the header. The DICOM standard defines more than 2000 attributes in the data dictionary, each of them encoding a particular item of information. The typical attributes are: a patient name, date, institute name, and much more. The scope of attributes depends on the study, the chosen modality, and the IT environment; it contains the specific information about real-world entities. The data dictionary (Part 6 DICOM Standard) can also be seen as a filter between a real world situation in a clinical examination and the abstract DICOM data encoding. [22]

As described, the basic information elements of DICOM are presented in the data dictionary. This consists of a so-called group code and an element code. In the standard, even-numbered group numbers are assigned without exception as the standard that implemented information elements. A complete tag element is composed as follows: | aaaa, bbbb |, where | a | refers to the groups and | b | belongs to the element identifiers. These identifiers can be used to uniquely identify all data elements in the data dictionary. Table 1 depicts the extraction of DICOM header elements from the recorded images.

DICOM Tag	Content
0008,0060	Modality: DX
0008,0068	Presentation Intent Type: FOR PRESENTATION
0008,1030	Study Description: Schädel ohne Processing
0008,103E	Series Description: Schädel ohne Processing
0018,0060	kVp: 57
0018,1050	Spatial Resolution: 0.148
0018,1153	Exposure in uAs: 25000
0018,1164	Imager Pixel Spacing: 0.148\0.148
0018,7004	Detector Type: SCINTILLATOR
0018,7008	Detector Mode: SingleShot1s
0018,702A	---: TRIXELL
0018,702B	---: PIXIUM2430EZ

Table 1. Image description based on the DICOM header

In detail, the data elements have their value representation (VR) and a specific VR length. DICOM-captured data has a large semantic range including millimeters, time, names, etc. which are recorded during a diagnostic process and many more clinical tasks. To maintain data integrity, this plurality of 27 basic data types is used. Each of these VRs is defined by a name including a definition, a permitted character set, and a maximum length. The identification of the VR is indicated by two letters in the DICOM standard paper. In the following example, the value representation “PN” has been used for the patient's name.

For example, `VR: Musterfrau-Mann^Maxima^^^Ph.D`

This syntax is understood by every DICOM-capable X-ray modality and can be processed semantically for clinical use cases like diagnosis, image processing, or image data presentation.

In DICOM, there are two different ways to define the length of a VR. One possibility indicated an explicit reference. Thus, the start- and end-points of the VR length can be defined. The second permissible variant is a fixed length specification for the VR. The length of the respective VR is predefined in the DICOM standard. Using this specification, the manufacturer must ensure that the maximum VR length is not exceeded. The consequences of a deviation from the standard would be a loss of DICOM conformity. The reason for the determination of the data length is the variance of the entries which can be different for the same data types such as "Name."

Based on the data dictionary, individual elements are grouped into objects. This is based on predefined structures. Several data elements from the dictionary build an accurately defined information unit. Furthermore, one or more objects can be embedded in a DICOM object. These objects are transmitted between the DICOM modalities and can be used for information exchange. [23]

Digital images or video recordings are integrated as data elements in DICOM objects containing all necessary information (attributes of the data dictionary). In a simplified representation, an object consists of the attributes row, column, and pixel data.

```
0028,0010 Rows

0028,0011 Columns

7EF0.0010 Pixel Data
```

In this structure, various images, video sequences, bio-signals, and many other digital data can be used in a DICOM object contained within a DICOM-capable IT environment. Data elements are combined into predefined semantically meaningful information blocks.

The DICOM standard defines blocks and subdivides them into modules, information entities (IE), or information object definitions (IODs). On the one hand, the modules form IEs, and on the other hand, these information entities build the IODs. Which modules would be used to build the IEs depends on the modality and clinical purpose of the data acquisition. The relationship and dependencies of the modules, IEs, and IODs are published by the NEMA.

Modules form the essential organization and basis of the metadata. The patient identification module includes all data elements such as patient name, PatientID,… to describe a real-world patient. For a module description, not all attributes are mandatorily needed. The stringent condition is that all the entered data elements should originate from the data dictionary and have to be encoded in a correct data type. If a video recording is embedded in a DICOM object, a corresponding module must be presented in the file header. This contains the required attributes for a correct playback of the video data—for example, the FrameTime (0018,1063). It indicates the time interval between individual images.

Some modules are obligatory (mandatory, M), while others only conditional (C) or can be defined by the user (user, U). The NEMA standard publishes whether a module is mandatory, conditional, or user-defined in DICOM part 3—for example, the patient identification module is mandatory. In that case, the patient is identified and the DICOM modality can create a name reference.

A defined set of modules forms a dedicated information entity. The DICOM standard provides different IEs such as a common patient IE or a common study IE. Thus, the common patient IE is composed of the patient module, specimen identification module, and clinical trial subject module. The common study module consists of the general study module, patient study module, and clinical study module. In the data structure, the IEs represent the next level of information and are built on the modules and data elements. Thus, an IE represents the facts of a real entity such as a patient in the DICOM header. The numbers and complexity of IE are constantly developed by NEMA.

DICOM information objects are defined information objects called IOD. These information entities are made up from several IEs and define a DICOM object. These information objects are also the central component in high-level DICOM communication. Modalities like computed tomography, magnet resonance tomography, or digital X-rays use IOD for data exchange.

A digital X-ray image (DX), including the corresponding information, forms a "DX-IOD." For comparison, a positron emission tomography (PET)-IOD originates from a nuclear medical imaging device that includes the image data and the related information. Some of the modules, such as a patient or general study, are equally used in both IODs. Other more specific modules, such as PET isotopes or DX detectors, are only shown in the respective IODs. Figure 14 depicts the screenshot of a DX image from the DICOM-viewer software with the related header information of a patient and the study IOD.

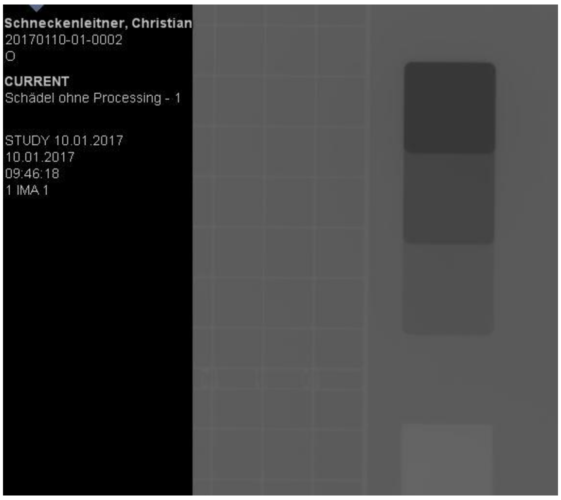

Figure 14. DICOM data representation and the related header information on the DICOM-viewer software

There are 27 value representations encoding data types in DICOM. Different types are identified by their VR name, the definition, the character repertoire and the length of the value. In the following, important value representations for pixel encoding have been described.

Depending on the purpose, the pixel data can be encoded in “Other Byte String (OB)” or “Other Word String (OW).” These two value representations are valid for overlay data and pixel data elements. The tag 7EF0,0010 is reserved for pixel data into the DICOM file structure. Furthermore, in case of the standard, the image data representation defined as attributes within the header of the file in different ways can be applied to the pixel data. Various X-ray modalities produce different datasets and bit depths—for example, a computed tomography system generates 12bit images, while an interventional angiography produces 16bit and planar X-ray systems, such as mammography or muscle skeleton modalities, take 12bit or 16bit radiographs. The requirement for the pixel data is that the current bit depth should be accommodated in a correct way. There are three data elements provided to ensure a proper structure.

bits allocated (0028,0100)

bits stored (0028,0101)

high bit (0028,0102)

During an acquisition process, X-ray exposition is done. This is captured by the detector system as a single pixel value. This recorded sample is encoded in a pixel cell. The size of each pixel cell is based and specified by the allocated bits (0028,0100), and the placement within the cell comes from the high bits (0028,0102). The pixel sample size is uniquely defined by the stored bits (0028,0100). The following is taken from the DICOM standard document part 5 and describes a pixel data encoding example.

> *For example, in Pixel Data with 16 bits (2 bytes) allocated, 12 bits stored, and bit 15 specified as the high bit, the one-pixel sample is encoded in each 16-bit word, with the 4 least significant bits of each word not containing Pixel Data.* [21]

Depending on the negotiated transfer syntax, the pixel data can be compressed or even not.

There are two different capabilities to transmit DICOM pixel elements. A native format is encoded without any compression methods or encapsulated formats defined outside the DICOM standardization workgroup. By using the native format encoding, the data type OW is applied. Alternatively, the OB value representation is used for encapsulated compressed formats. The supported methods are JPEG image compression, run length encoding (RLE) compression, JPEG-LS compression, or JPEG 2000 image compression. For video encodings, MPEG2 MP@ML image compression, MPEG2 MP@HL image compression, or MPEG-4 AVC/H.264 High Profile/Level4.1 video compression are available. [21]

2.2.2 Processing and analyzing with ImageJ

ImageJ is a platform-independent image processing and analyzing software. It focuses mainly on medical imaging. The java-based program was mainly developed by Ryan Rasband from the National Institute of Health (NIH). The open architecture allows a broad spectrum of user groups to develop plugins for their issues. [24].

The up-to-date software download is available on the website:

https://imagej.nih.gov/ij/download.html

2.3 Data visualization and dashboard design

Regarding Munzner [25], a data visualization process can be divided into three parts. The main questions are “what” data is being represented to the user, the main intention to do this, and “why” the user needs it the way in which the data is visually encoded. This question-framing process of “what-why-how” leads to data-task idioms. Visual perception is done by the human eyes and includes the reception and processing of visual singles from the environment. Visual analytics in healthcare environments is a current scientific topic.

Dashboard development in medicine and in the field of radiology is a scientific subject. Furthermore, commercial data analysis and visualization software products, such as Tableau, focus on healthcare [26]. Therefore, many design protocols and development of example cases have been published over the last decade. A well-defined dashboard design and development process are needed for an effective implementation.

> *Data is prolific, but usually poorly digested, often irrelevant and some issues lack the illumination of measurement.* [27] *(1970, p. 466)*

This quote from John D.C. Little [27] in the early 1970s can be found in various publications and underlines the importance of this topic. As described in “models and managers” by Little, most working groups focus on the economic aspects.

Other main subjects in the field of medicine are patient safety and patient care. For medical dashboard application, two different definitions can be found, namely quality dashboard and clinical dashboard.

A quality dashboard can be described as:

> *Health IT that provides a visual display of quality or productivity indicators (metrics) to enable managers at the organizational and/or ward/unit level to identify areas of practice for improvement.* [28]

On the contrary, a clinical dashboard is defined as:

> *Health IT that provides a visual display of quality or productivity indicators to individual clinicians to "provide clinicians with the relevant and timely information they need to inform daily decisions that improve the quality of patient care." They may provide data at the level of the patient and at the level of the healthcare professional (showing all patients that they are being cared for and then comparing them with their peers and national benchmarks) or may allow the user to move between viewing information at both these levels.* [28]

The clinical dashboard definition is taken from Dowing et al. [28]. It is based on the primary literature from the network of health services (NHS) [29] and Linder et al. [30].

Dowing et al. [28] have focused in their literature review on dashboards to improve patient care; they have identified 11 scientific publications between 1996 and 2012. Overall, nine of these reasearch works focus on health professionals as the targeted intervention group. Particularly, the study by Morgan et al. [31] was in the field of digital radiology and medical imaging. As many as 47 radiologists within the department was named as the intervention group. Summarized, the dashboard was integrated in the PACS workflow, and significant differences in the turnaround time were measured without and with the dashboard.

Effective implementation within the radiology department is essential for dashboard development. The key findings of Karimi et al [32] considering organizational culture, determining the goal of dashboard design, involving users, aligning them with organizational goals, determining key performance indicators and benchmark standards, data, knowledge discovery, security, flexibility, timeframe, representation, and dashboard evaluation are crucial for successful design and development.

Karami et al. [33] have introduced a design protocol to develop a dashboard for the radiology department. The scientific group determined four major steps to design and develop a dashboard and described it in a descriptive manner.

1) Determine the key performance indicators for radiology
2) Determine a comprehensive model for the designing of dashboards
3) Determine the required infrastructure for the implementation of radiological management dashboards
4) Determine the key criteria for assessing the dashboards

3 Image Processing, Analysis, and Visualization

The methodological realization to build a visualization toolkit for an image quality assessment dashboard was divided into different work packages, namely the data acquisition process and the preprocessing task. Following this, the feature extraction and local contrast calculation were performed. In the final data-processing step, the metrics were transformed into a visualization toolkit to provide an image quality dashboard for expert evaluation. In this chapter, the procedures will be described and well documented.

3.1 Digital image acquisition process

A commercial DR imaging system and X-ray unit were used to generate raw images from a phantom structure plate.

The Philips “Optimus 50” X-ray generator and the Philips “BuckyDiagnost” X-ray unit performed the imaging. During the whole process, some parameters were fixed and others were changed in a well-known manner. To ensure optimal geometrical properties, a small focal spot was chosen for all images. The source-detector distance was fixed at 120cm. For the X-ray exposure, no scatter grit was used and an over-the-table method was performed. The experimental positioning setup was based on classic examinations like antebrachial or leg studies.

The X-ray detector for image generation was a Philips “sky plate” wireless system. An absorption area of 24cm/30cm defines the active field of view for the detector plate. The indirect conversation method with the Natrium Iodine scintillator material produces a visible light signal. The data processing inside the detector was done by a trixell pixium 2430EZ. The amount of signal and the distribution are registered on the thin film transistor (TFT) matrix and converted into a digital 2D matrix.

The measured signal and the digital gray value are linearly related and express the photon absorption behavior of the imaged object under certain physical conditions. This projective representation is the raw image dataset with a pixel depth of 16 bits. The trixell pixium A/D converter produces 65.536 differentiable values and describes the intensity distribution on the detector plate in a digital manner. By changing the acquisition parameters, namely kV and mAs, different digital raw images were produced. This data builds the base to measure and calculate the contrast over the image cluster.

For clinical interpretation, an image adjustment is automatically performed by a software package. The use of these processed images was not the goal of this work. Figure 15 pictures the imaging acquisition process from the X-ray unit to the raw image which was used to measure and calculate the primary contrast metrics.

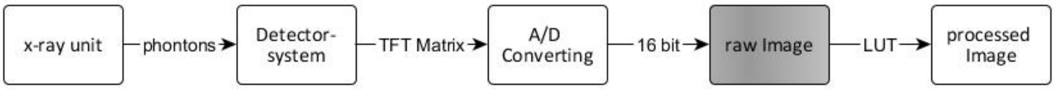

Figure 15. Input–output flowchart

All detector specifications for raw image data are shown in Table 2.

DICOM Tag	Content
0008,0060	Modality: DX
0008,1030	Study Description: Schädel ohne Processing
0008,103E	Series Description: Schädel ohne Processing
0018,1050	Spatial Resolution: 0.148
0018,1164	Imager Pixel Spacing: 0.148\0.148
0018,7004	Detector Type: SCINTILLATOR
0018,7008	Detector Mode: SingleShot1s
0018,702A	---: TRIXELL
0018,702B	---: PIXIUM2430EZ
0028,0002	Samples per Pixel: 1
0028,0010	Rows: 1499
0028,0011	Columns: 1888
0028,0100	Bits Allocated: 16
0028,0101	Bits Stored: 15

Table 2. Detector description based on the DICOM header file

The used imaging modality was a digital X-ray system (DX). The conversion process from X-ray photons to visible light was performed by a scintillator material. Every single exposure produced an image on the detector plate (0018,7008). The TFT matrix was created by 1499 rows and 1888 columns on an active surface of 240mm x 300mm. For each TFT element, one sample (0028,0002) with a depth of 16 bits was quantized (0028,0100). The resolution on the TFT detector element (Del) was 0.148mm (0018,1050) and the pixel element spacing (0018,1164) corresponds to the detector dimension. During the image generation process, a 1:1 binning was performed by the detector system. In this case, every TFT-Del is converted into a pixel element and the TFT matrix size is equal to the image matrix size. The files were exported without any image processing as raw intensity data (0008,1030, and 0008,1030E).

3.2 Image cluster with various acquisition parameters

To ensure good reliability and exclusion of the possibility to succumb to random measured values, a series of test images under the same acquisition parameters was received. For this purpose, 10 X-ray images with 57kV and 109mAs were taken from the phantom test pattern.

The image cluster is defined as a matrix of rows and columns containing local contrast items over the total range of acquisition parameters. During the actual data-recording process, raw images with different photon energies were taken. By varying the kV over to a whole range of possible options, an array of images with different energy spectra was produced. For each kV, different images with varying mAs were taken. Eventually, an image cluster with various kV and mAs was produced, thus allowing the analysis of contrast for multiple features in each image. A 2D array of 12 different energy spectra images from 57kV to 109kV with seven different mAs levels from 10mAs to 40mAs built the initial dataset. Figure 16 pictures the 84 images within the image cluster.

Each image distinguishes a characteristic contrast behavior, depending on the used kV and mAs. The assessment was performed with certain image-processing techniques.

		kV											
		57	60	63	66	70	73	77	81	85	96	102	109
mAs	10	1	2	3	4	5	6	7	8	9	10	11	12
	12.5	13	14	15	16	17	18	19	20	21	22	23	24
	16	25	26	27	28	29	30	31	32	33	34	35	36
	20	37	38	39	40	41	42	43	44	45	46	47	48
	25	49	50	51	52	53	54	55	56	57	58	59	60
	32	61	62	63	64	65	66	67	68	69	70	71	72
	40	73	74	75	76	77	78	79	80	81	82	83	84

Figure 16. Image cluster matrix and acquisition parameters

3.3 Image-processing pipeline for feature extraction

The image processing and analysis were implemented and realized as a plugin in ImageJ. Different methods were used to standardize the measurements and extract information from different areas within the images.

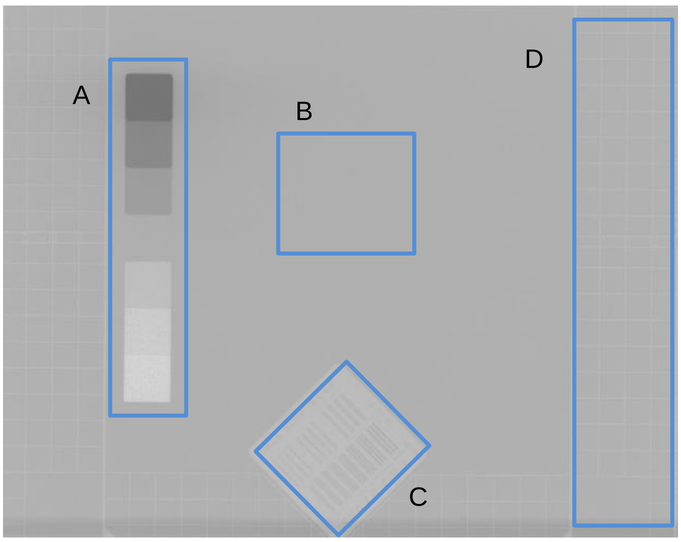

Figure 17. X-ray test pattern with different quality domains; A. contrast; B. homogeneity; C. spatial resolution; D. geometrical behavior

An X-ray raw image is shown in Figure 17. This X-ray test pattern is divided into different quality assurance domains: A. is used to measure contrast behaviors; B. is suitable for homogeneity testing; in C. spatial resolution can be measured; and the grid bars in D. carries geometrical information to the imaging system. For the current work, the seven intensity scales in Area A. were used. Figure 18 pictures the phantom plate that was used to generate the X-ray images.

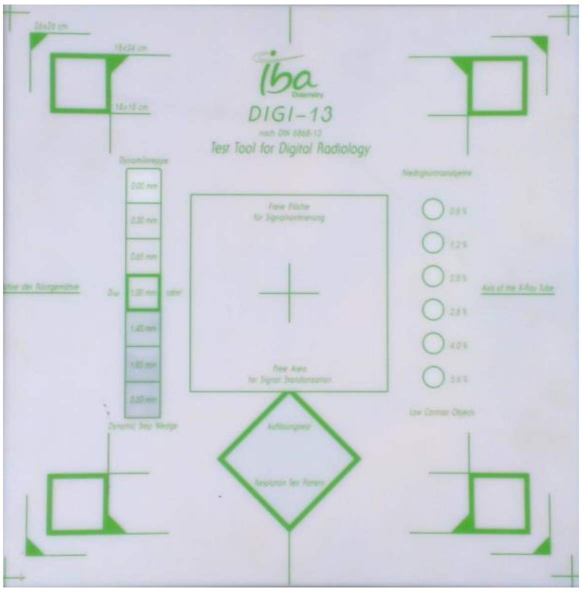

Figure 18. Digi 13 phantom plate: A test pattern for radiology

Within the scope of the pre-test phase, all features within Area A were used to consider a stable, solid test environment. With a set of 14 images, a reliability test was carried out. A low kV series with 48kV and a mid-energy series with 77kV were performed. A series is made up of seven images under same acquisition parameters. The goal of the pre-test was to verify stable image quality within the features. Figure 19 pictures the ROI position from which the intensity distribution metrics were measured. From each image, all seven features were used to represent a good cross-section of the signal intensity over the X-ray energy spectra and attenuation behavior in the radiographs.

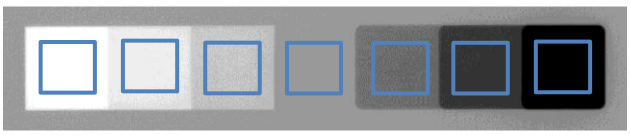

Figure 19. Progressive intensity scale: The blue ROIs mark the measurement area in the feature

The pixel raw values inside the ROI area were recorded and calculated. All the metrics were computed by standard imaging methods from the ImageJ library. The ROI manager and the stack measure ImageJ function ensure a steady and controlled data-generating process.

Following this, all single images within the image cluster were taken to gather, measure, and calculate the contrast behavior. Before the image processing, all the images were brought together in a file folder. ImageJ used this as the image source for further patch-processing. The X-ray test pattern images had the same structures in corresponding areas over the whole stack. This ensured that all the measured metrics were raised from equal areas.

To identify and separate different images, a logical consistency of renaming was followed manually for all images. All the files were named by the numbers of used kV and microampere seconds. This ensured a controlled data extraction process and an explicit association over all the measured features within the image stack. To make sure that the images are handled as DICOM files, the suffix ".dcm" was applied to all files. Figure 20 depicts the folder with all DICOM images in the renamed structure.

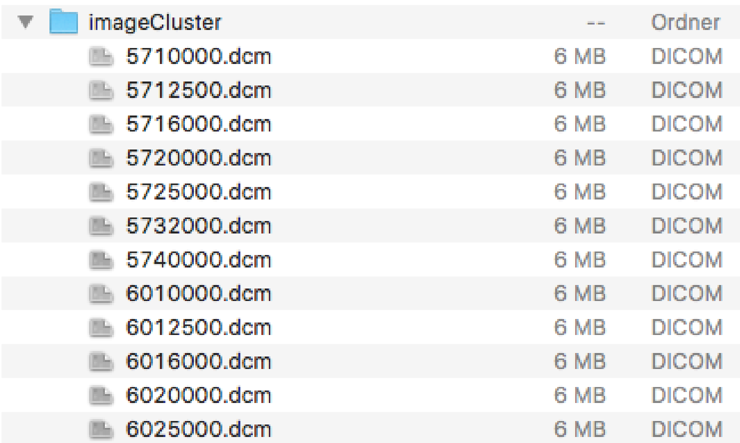

imageCluster	--	Ordner
5710000.dcm	6 MB	DICOM
5712500.dcm	6 MB	DICOM
5716000.dcm	6 MB	DICOM
5720000.dcm	6 MB	DICOM
5725000.dcm	6 MB	DICOM
5732000.dcm	6 MB	DICOM
5740000.dcm	6 MB	DICOM
6010000.dcm	6 MB	DICOM
6012500.dcm	6 MB	DICOM
6016000.dcm	6 MB	DICOM
6020000.dcm	6 MB	DICOM
6025000.dcm	6 MB	DICOM

Figure 20. Image cluster folder with structured and renamed DICOM files: The first two numbers denote the kV and the last five the µAs

The image quality calculation was carried out over seven intensity steps per image. Regarding that, seven ROIs for 84 different images in the image cluster were taken to calculate the primary quality metrics. In that case, 588 ROIs were extracted. The orange numbers in Figure 22 picture the available intensity steps within an X-ray image. To calculate the image contrast behavior, the intensity neighbors were chosen. Contrast 1 can be calculated by analyzing Intensity Steps 1 and 2, while Contrast 2 was generated by the information gathered from Intensity Steps 2 and 3. Overall, six types of contrasts could be acquired by the seven intensity steps. The blue numbers in Figure 21 depicts the contrast capabilities for one X-ray image.

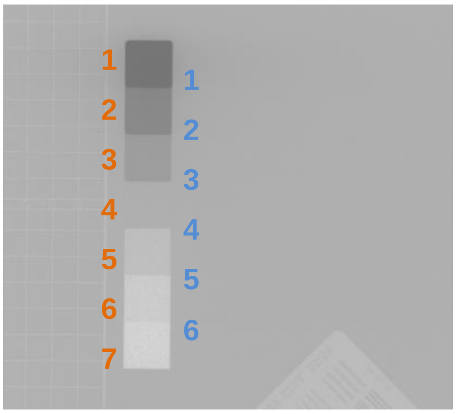

Figure 21. X-ray test pattern.

Intensity and contrast steps were packed into a stack. Features with different intensity levels over the whole gray value spectrum were identified and regions of interest were drawn.

The image-processing pipeline is elaborated in a flow diagram and divided into different logical steps.

Step 1 Manual preparation

Step 2 Image to stack

Step 3 Set ROIs into features

Step 4 Set measurement and measure stack

Step 5 Save metrics as results

Step 1 was described earlier. The images were manually renamed by kV and mAs and then copied into a folder. In Step 2, all images within the folder were opened in an ascending order and formed to stack. The ImageJ function “stacks” is used to display the related single image in a stack. All 2D images are linked as slices by increasing the number of kV and mAs for processing. This stack forming procedure is the default method of this function. Figure 22 pictures the process within the software.

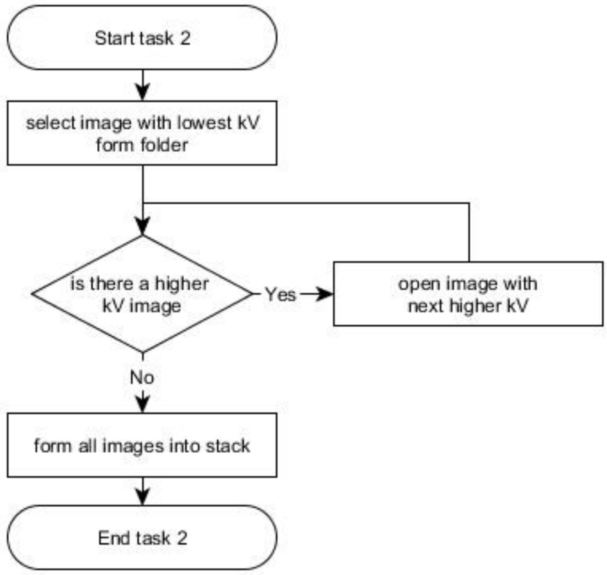

Figure 22: Flow diagram image process: Task 2

The next work task was the region of interest (ROI) placement on the contrast features. The function "setROI" and the ROI manager tool were used to capture the metrics within all images as well as features for the whole stack. Figure 23 is a schematic workflow picture from Task 3.

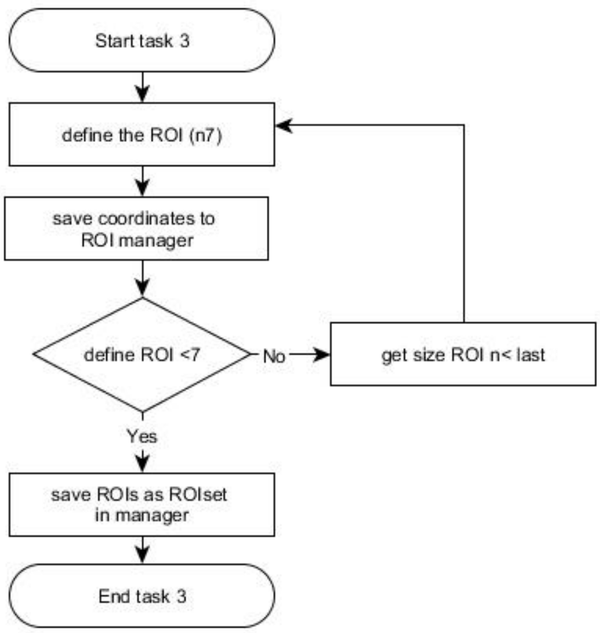

Figure 23. Flow diagram image process: Task 3

This procedure ensured that all ROI sizes and placements were equal to the overall measurements for metric extraction.

Task 4 contains the settings and measurements for the raw metric from the image cluster. The first work step was done manually and includes the selection of the measured quantities. For the measurement process, the function “measure stack” was used to extract the data from the ROIs. The flow chart in Figure 24 illustrates this image-process task.

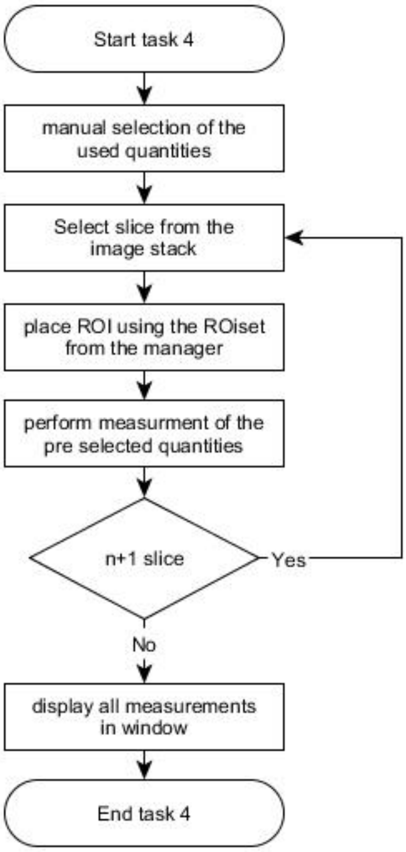

Figure 24. Flow diagram image process: Task 4

The last step within the imaging pipeline was done manually. The measured metrics were saved as comma separated (csv) files. To identify the measured images and features, different columns were defined. Table 3 is showing the header structure and one row in a table format. Stack:ROI1 refers to the image cluster, with the first two numbers representing the used kV and the last five numbers being the µAs product of the image. In Table 3, the results from the stack image with 57kV and 10000 µAs, including all ROI measurements (1–7), are shown.

Image Label	ROI1	ROI2	ROI3	ROI4	ROI5	ROI6	ROI7
Stack:ROI1:5710000	27474	26615	24945	22942	20744	18085	15608

Table 3. Structure of the comma separated file

This raw table includes all 84 image measurements from all the features in a row.

The local contrast calculation was done after the csv import by Excel 2010. All intensity neighbors 1–2, 2–3, 3–4, 4–5, 5–6, and 6–7 were used to compute the numerical local contrast metric.

3.4 Visualization tools for quality assessment

The goal of the visualization process was to simplify the image raw data in keeping with the needed numbers of quality metrics. In general, the data abstraction of radiographs is based on a numeric interval-scaled data type. The raw or input data is gray value based on the measured detector intensities. The grey level and thus the detector intensity is based on attenuated photons passing through an object. The analog-attenuated signals are digitally converted and coded in a 2D matrix as numeric values. The visualization represents the intensity differences in predefined regions. In the current use case, the contrast behavior for all images over the range of acquisition parameters was implemented.

3.4.1 Raw data description

The measured and extracted image raw data from the detectors system was coded in Unit16. The numeric range reaches from 0 to 65.535 numbers. Within this range of numbers, all quality metrics were calculated. To be annexed, Table B pictures the raw metrics of all 84 images including the minimum value, the maximum value, and mean values. The absolute numbers for all the images are shifting depending on the primary acquisition parameters caused by increasing the mAs product. Table 4 pictures the extreme values of mean and standard deviation within the image cluster for the whole image content, and the feature extraction area gives a raw picture. While increasing the kV parameter, the standard deviation decreases from 3999 in the ROI area as well as from 3174 in the whole image content to 1065 in the ROI and 1357 in the whole image content. Table C in the Appendix shows all mean and standard deviation values for all images within the image cluster. This ordered table gives some indications of the data situation for further contrast calculation. A minor standard deviation indicates a smaller range of grey values and might influence the local contrast behavior for the features.

Measurement		Results
Minimum mean	ROI	8093
Maximum mean	ROI	22341
Minimum mean	All	7880
Maximum mean	All	22705
Minimum StdDev	ROI	1065
Maximum StdDev	ROI	3999
Minimum StdDev	All	628
Maximum StdDev	All	3174

Table 4. Mean and standard deviation for the whole image and the featured area calculated from the grey values

This numeric fact is well-founded in the physical nature of photons, which interact with matter. Moreover, all local differences exhibit in a correct manner. According to that, the visualization of local contrast is valid for the whole images cluster. Table 5 depicts the contrast metrics for all kV steps for 10mAs and 40mAs. In the two metrics, the local contrast decreases while increasing the photon energy under the same conditions.

mAs	57kV	60kV	63kV	66kV	70kV	73kV	77kV	81kV	85kV	96kV	102kV	109kV
10	859	853	821	802	751	719	682	643	611	535	498	466
40	829	823	814	786	746	715	680	638	601	524	493	443

Table 5. Local contrast metrics for all kV steps for 10mAs and 40mAs

3.4.2 Visualization elements for the quality dashboard

A supportive information and orientation field, a dashboard header, and the main information field were compounded to a dashboard. These three main fields were subdivided into different elements.

No colors were used to design the background elements. Colors were only used to set hints, visual relations, or coding the image quality within the local contrast tables.

The used elements in the supportive information field were used to picture the intensity step with the calculated local contrast and the color scale for the contrast tables. To do this, the intensity scale and the numbers of local contrast were presented.

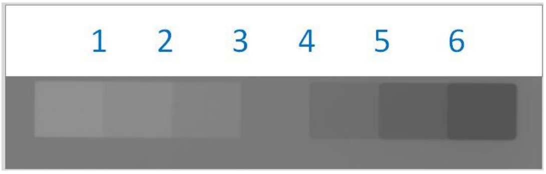

Figure 25. Contrast step elements for the image quality dashboard

Figure 25 illustrates this visualization element. The blue numbers refer to the six calculated contrasts over the seven intensity steps.

To define a minimum, the maximum and the color gradient were provided. These elements were designed with reference to the color tables. Figure 26 pictures the elements with a description of minimum and maximum contrasts.

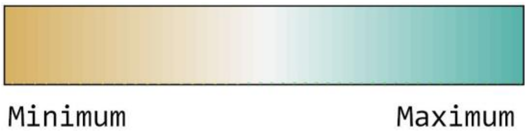

Figure 26. Color gradient for the image quality dashboard

The image quality tables are located in the main dashboard field and represent the largest area. This field was subdivided into six areas, each containing the table for one local contrast step. To separate the different steps, an information box was used. Each box provides the local contrast and highlights the corresponding step. A correlation between the contrast step elements in Figure 25 and the contrast table identifier was given by the blue labeled numbers. Figure 27 pictures the table identifier for Contrast Step 1.

Figure 27. Contrast table identifier for the image quality dashboard

The color tables within the local contrast information were built on the extracted and calculated image feature by measuring the defined ROIs. The raw data was arranged in a pre-structured cluster. The rows include the kV data for all acquired radiographs and the columns were used to record the mAs Product. Within this cluster, all calculated local contrast data was listed.

mAs	57kV	60kV	63kV	66kV	70kV	73kV	77kV	81kV	85kV	96kV	102kV	109kV
10	859	853	821	802	751	719	682	643	611	535	498	466
12.5	846	846	817	794	751	724	680	644	608	532	497	464
16	836	845	825	793	751	721	679	641	611	528	494	464
20	836	838	818	798	753	722	676	643	609	527	494	464
25	845	841	819	795	747	715	678	644	608	524	495	463
32	823	830	818	791	750	714	680	642	604	524	493	462
40	829	823	814	786	746	715	680	638	601	524	493	443

Table 6. Raw contrast values for the quality assessment cluster in the first contrast step

Table 6 pictures the cluster structure and the numeric values containing all images with the acquisition parameters. For a better readability, the header row and first column describe the parameters by name.

For the conversion of the calculated numbers into colors, the online platform ColorBrewer2.0 was used [34]. This website provides different predefined colored maps and configuration capabilities. The main visualization focus is on the field of coding colors in cartography. Figuratively, the generated image cluster is a parameter map for detector contrast behavior. The color-based distinction was based on three main color classes. An additional requirement was that these classes are safe for colorblind people. have to be colorblind safe.

Color	r	g	b
	90	180	172
	245	245	245
	216	179	101

Table 7. Color classes for contrast visualization

Table 7 pictures the main color classes and the associated RGB code. In ColorBrewer, the nature of the data has to be defined. The main aim of the visualization toolkit is to distinguish high from low contrasts. This approach refers to the identification of a divergence in the dataset. The chosen color types lead to the separation of the dataset and provides a good basis for decision-making.

The color assignment for the decided contrast metrics was performed for each contrast table separately. The local contrast minimum and the maximum were identified for each table, and the RGB code was accordingly assigned. Color class one r90|g180|b172 is used for the maximum, while color class three r216|g179|b101 represents the minimum contrast for the color table. The color class two divided the dataset into higher and lower contrast parts. To determine the data distribution, the statistical quantile $Q_{0,5}$ was calculated. The RGB color code for the second class was placed on $Q_{0,5}$. Starting from this calculated values, a linear color gradient was applied for all contrasts.

Table 8 pictures a single contrast table. The columns represent the photon energy expressed in kV, while the rows represent the amount of signal in mAs. By reading the table row-wise, the contrast behavior for a specific mAs step with different kV can be identified and compared. Conversely, each column contains the contrast behavior over the acquired kV step for different mAs images.

The color gradient is valid for one contrast table. All calculations are carried out for each contrast step separately. Any table contains their own minimum, maximum, and $Q_{0,5}$. In this visualization manner, different tables should be compared carefully. Table D in the appendix presents the local contrast and the whole feature contrast. This illustration pictures the different types of color coding based on diverse minimum, maximum, and $Q_{0,5}$ calculation.

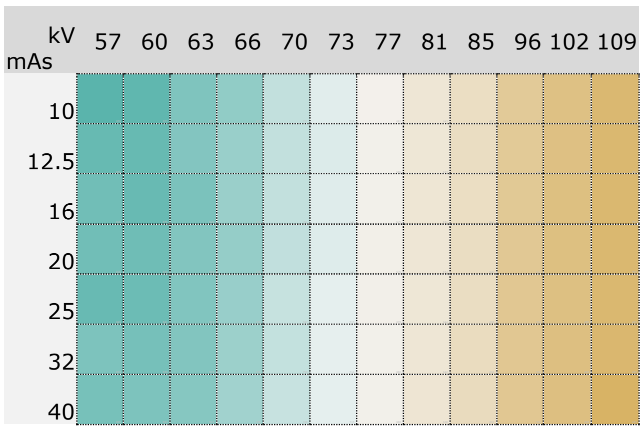

Table 8. Color map for contrast behavior at the first contrast step

All the tables are arranged as small multiples of the main local contrast area within the image quality dashboard.

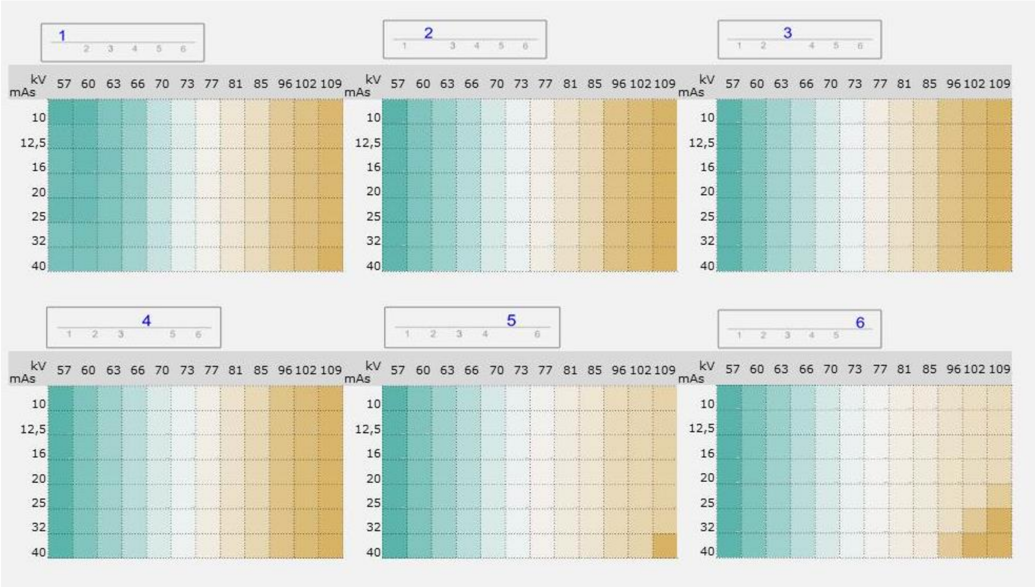

Figure 28 Contrast color field within the image quality dashboard

In Figure 28, the contrast tables are sorted into three columns and two rows. The first row includes the Contrast Steps 1, 2, 3 and the second row holds the Contrast Steps 4, 5, 6.

4 Metric Calculation, Validation, and Dashboard Evaluation

This chapter contains all the results and findings from the processing and analyzing work tasks. All the results are ordered in a logical manner and confirm the work tasks from Chapter 3. In Subchapters 4.1 and 4.2, the numeric results of the image processing are pictured. In Chapter 4.3 the image quality dashboard is presented. Chapter 4.4 contains the dashboard evaluation and analysis.

4.1 Feature reliability measurement

To verify stable gray values from the features, a series of 14 images was taken to calculate the mean, the standard deviation (StdDev), and the standard error of the mean (SEM).

The raw measurements were done with ImageJ by defining ROIs into the features. A mean gray value, standard deviation (StdDev), and minimum and maximum metrics were extracted. A calculation of the standard error of the mean was calculated from each feature from a total of seven images per kV step. In the following, the pseudo code illustrates this process.

```
public class _StdROIMeasurement_Plugin implements PlugIn {
  public void run(String arg) {
    ImagePlus imp = IJ.getImage();
    RoiManager rm = RoiManager.getInstance();
    if (rm==null) rm = new RoiManager();
    rm.select(0);
      IJ.run(imp, "Measure Stack", "");
    rm.select(1);
      IJ.run(imp, "Measure Stack", "");
    rm.select(2);
      IJ.run(imp, "Measure Stack", "");
    rm.select(3);
      IJ.run(imp, "Measure Stack", "");
    rm.select(4);
      IJ.run(imp, "Measure Stack", "");
    rm.select(5);
      IJ.run(imp, "Measure Stack", "");
```

```
      rm.select(6);
        IJ.run(imp, "Measure Stack", "");
      IJ.saveAs("Results",
"\\\\algedvsv14\\home_alg\\c.schneckenleitner\\Desktop\\
StdResults.xls");
   }
}
```

The results mirror the attenuation effect for the different features. Within the measurement range, the SEM metric, and consequently, the photon attenuation from ROI 1 to ROI 7 follows a tendency. The lower is the material thickness, the lower is the expected standard error. This effect can be seen in both energy domains. The scale is different and can be found in different attenuation influences for 48kV and 77kV. The higher X-ray images taken with 77kV are affected less by photon absorption and provide a more homogeneous distribution on the detector system. A theoretical estimation of the SEM based on gray values is shown in Table 9.

kV	Feature	Standard error of the mean
48kV	1	491.73
	2	506.36
	3	371.65
	4	120.25
	5	56.37
	6	30.94
	7	11.72
77kV	1	15.82
	2	14.63
	3	12.47
	4	9.23
	5	11.61
	6	9.56
	7	6.43

Table 9. Reliability testing for the feature metric with mean, standard deviation, and standard error of the mean

Table 10 allows more detailed analyses of data stability among the single measurements for specific features. The table pictures the ROI1 data. The total numbers of measurements are annexed and shown in Table D. The measurement of variation, expressed as standard deviation and standard error, represents the data estimation. The two parameters were solid for 48kV and 77kV radiographs.

Label	Mean	StdDev	Min	Max	Slice	SE	SEM
ROI1:4810001	31124	1318	27940	32767	1	498.16	
ROI1:4810002	31303	1294	27650	32767	2	489.09	
ROI1:4810003	31256	1312	27877	32767	3	495.89	
ROI1:4810004	31249	1304	27743	32767	4	492.87	491.73
ROI1:4810005	31283	1297	27889	32767	5	490.22	
ROI1:4810006	31275	1302	27877	32767	6	492.11	
ROI1:4810007	31335	1280	28044	32767	7	483.79	
ROI1:7725001	14664	42	14518	14802	8	15.87	
ROI1:7725002	14660	42	14515	14793	9	15.87	
ROI1:7725003	14661	42	14493	14783	10	15.87	
ROI1:7725004	14660	42	14487	14783	11	15.87	15.82
ROI1:7725005	14663	41	14489	14796	12	15.50	
ROI1:7725006	14660	42	14504	14799	13	15.87	
ROI1:7725007	14660	42	14508	14776	14	15.87	

Table 10. Mean, standard deviation, and standard error of the mean from the pretest images

4.2 Local contrast calculation from the radiograph features

The local contrast calculation was systematically performed for all images and features by ImageJ and Microsoft Excel 2010. In the pretest phase, the reliability was ensured and the contrast calculation could be carried out.

Schematic results for two local contrast steps ROI1 and ROI2 are shown in Table 11. For each kV range, seven different mAs images were taken and analyzed. The total number of contrast for all images is annexed in Table E and provides the initial contrast data.

Label	ROI1	ROI2	Contrast1	ROI2	ROI3	Contrast2
Stack:ROI1:5710000	27474	26615	859	26615	24945	1670
Stack:ROI1:5712500	26876	26030	846	26030	24373	1657
Stack:ROI1:5716000	26213	25377	836	25377	23722	1655
Stack:ROI1:5720000	25610	24774	836	24774	23126	1648
Stack:ROI1:5725000	25054	24209	845	24209	22556	1653
Stack:ROI1:5732000	24395	23572	823	23572	21924	1648
Stack:ROI1:5740000	23827	22998	829	22998	21355	1643

Table 11. Local contrast for Steps 1 and 2

4.3 The dashboard for image quality assessment

The aim of the visualization toolkit was to picture the total contrast situation from the acquired radiographs on one single page. Figure 29 pictures the dashboard mock-up.

The imaging dashboard is divided into the header, an additional information part, and the main contrast visualization box. The most ancillary information elements are placed on the left section of the dashboard. In this area, the user can find a screenshot of a representative X-ray and mark contrast steps by the numbers from 1 to 6. This element is designed to give a visual support to the intensity distribution and gray value; it represents a conjunction between quality visualization and a taken X-ray image. Using this, a user can match the gray value and the contrast metrics in the contrast cluster of interest.

The lower part of the additional information part displays the color code and the used gradient for minimum and maximum contrasts. The main area is the image quality assessment box within the contrast data over the whole cluster.

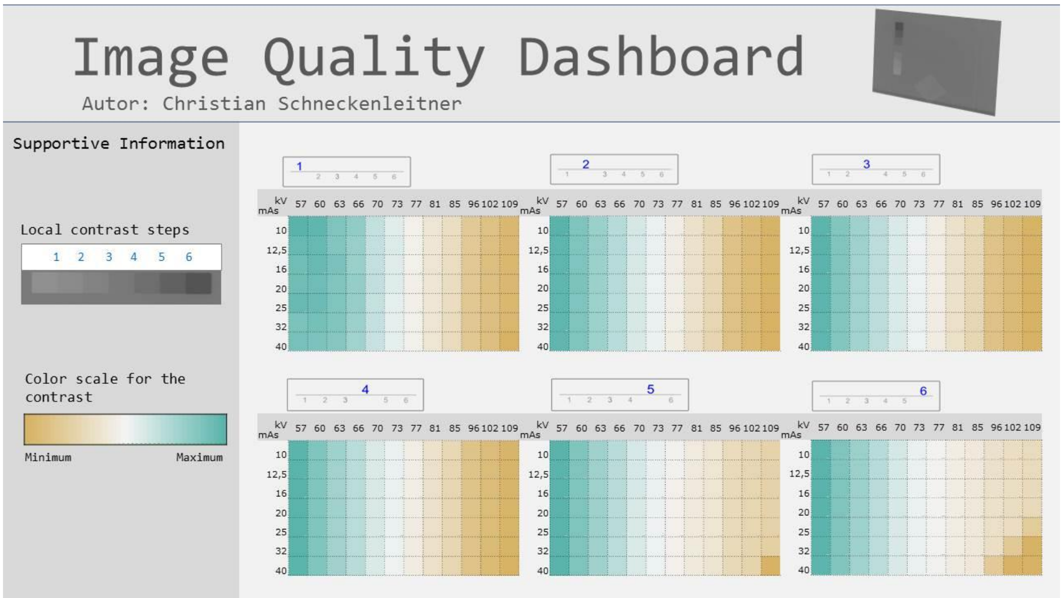

Figure 29. Image quality dashboard overview

4.4 Dashboard evaluation and analyses

An analysis based on scientific standards in the field of image quality assessment in digital radiograph was executed. Following this, an empirical dashboard evaluation was realized as a structured expert interview. The dashboard design and analysis were performed by “a comprehensive model for designing the radiology dashboard” developed by Karami et al. [33]

4.4.1 Scientific findings for image quality assessment

According to the empirical findings by Williams et al. [16], three core statements are pertinent to the current work to use a digital X-ray system. The gray text lines are statements from the scientific literature. The mock-up analysis is described in the following.

a) *The availability of image-processing stations and evaluation programs to improve the analysis*

Image-processing workstations are available for any digital detector system. Conversely, analysis programs to improve the image quality are not implemented during clinical imaging processes.

The work connected the key elements for performing a high-quality digital radiograph.

a) *Development of secure acquisition protocols to ensure image quality and radiation dose independent of the examination room and the used workstation.*

   Image quality dashboards visualize local contrast situations and support radiographers by choosing the ideal acquisition parameters for their specific clinical use case.

b) *The possibility of image processing to represent a higher quality of the acquired information*

   Raw data processing and analysis to assess local contrasts within radiographs under certain acquisition parameters provides the possibility of high-quality images.

c) *Minimize the occurrence of poor X-ray image quality*

   The dashboard prototype predicts local contrast situations in radiographs under certain acquisition parameters and minimizes unexpected poor X-ray image quality.

d) *The establishment of a clinical quality development*

   Experts with background knowledge were integrated in the evaluation process. Five questions were formed in connection with the usefulness of the prototype.

4.4.2 Results from the structured expert interview

The test phase was targeted on experts to determine the usefulness of the quality assessment for the developed dashboard elements. The inclusion criteria for an expert were predefined in the following way.

- Work experience in a university field
- More than 10 years of experience in medical imaging
- Ph.D. or MSc degree in the field of physics or medical imaging

The low executed mock-up of an image quality dashboard should support the radiographer to estimate local contrast behavior in X-rays. The aim of this work task was to provide solid results for the visualization toolkit and to validate the usefulness of the mock-up dashboard. Therefore, a test environment and the methodological procedure were created.

All dashboard elements were created with different software packages and frameworks. The arrangement for the test set was done with a PowerPoint slide. This ensured the fact that all experts would be able to open the dashboard in an easy and simple way on their monitors. A minimum screen resolution requirement of 1920x1080 to be displayed on the monitor was preconditioned.

The dashboard should pose in a full-screen mode. This ensured that the dashboard would be shown in the full monitor resolution.

The open questions was formed to identify the usefulness and determine further improvements. In the document header, the tester described experiences in the field and test settings. In the following, the phrased questions are listed.

1. This question refers to the perceived usefulness and represents the perspective probability of a user increasing the job performance and improving the quality of work.

   Do you think that this dashboard would increase job performances for radiographers? Say yes or no and then explain your decision.
2. The main interest is the perceived ease of use*. Is the color representation of the quality criteria (local contrast) easy to use?*

3. The use of new technologies underlies external factors.
   Which external variables can or may influence the acceptance for radiographers?

   a. b. c. d.

4. Patient risk and misleading the patient is a critical point for the quality toolkit.
   Does it lead the visualization to a misleading interpretation or patient risk? Answer in yes or no and then give the reason for the answer.

5. Some questions about the dashboard.
   Provides the dashboard with all necessary information or does it get overloaded in any way?

The document and email text are annexed in Figure D. The questionnaire and the image quality dashboard slide was transmitted via email and the answers were received in a digital way.

The implemented expert determination is based on open questions and then compared with scientific background knowledge. The pivotal elements in digital radiograph acquisition and image quality constitute the main purpose of this subchapter.

In the following, the expert feedback is shown in the entire text lines. The capitals (A and B) denote the expert answers.

1. Do you think that this dashboard would increase job performances for radiographers? Answer in yes or no and then explain your decision.

A: *This dashboard shows the contrast between the pictures depending on kV and mAs settings. Radiology-technologists can make the measurements with their equipment in accordance with your dashboard to create a new one for their use case.*

B: *Yes,*
The Dashboard may increase job performance mainly in the introduction phase of new Equipment, process of implementation of new Studies and protocols, as well as for the regular Quality control of Images and parameters

2. Is the color representation of the quality criteria (local contrast) easy to use?

A: *The color representation of the quality criteria can be used. But I would rather have represented it in the gray scale because radiologists are used to look at radiographs and evaluate them through the gray scale.*

B: Yes, Nevertheless explanation of supportive Information may increase the understanding.

3. Which external variables can or may influence the acceptance for radiographers?

A:

a. Simple,
b. Short,
c. Understandable
d. A discussion forum

B:

a. Institutions awareness of Image quality control

b. Affinity of Staff for technical issues

c. Time Resources

d. Adequate Infrastructure

4. Leads the visualization to a misleading interpretation or patient risk? Say yes or no and give some reason.

A: *No, because radiologists are technically able to correctly interpret the information on kV, mAs, patient dose, and image quality.*

B: *No, Nevertheless instruction and exercise with the toolkit is strongly recommended*

In my point of View Radiographers would mainly tend to check which mAs setting will not bring additional contrast for the required image Quality

5. Provides the dashboard with all necessary information or does it get overloaded in any way?

A: *It is, of course, necessary to understand the system behind the dashboard before using it. But once the user gets to understand how to use the dashboard, the image quality would increase, and at the same time, the risk of unnecessary patient dose would decrease.*

B: Yes it provides all information necessary.

The representation of interaction of 4 Variables in a Dashboard (mAs, KV, Contrast Step, and color-scale as a result) is complex and has to be well understood first by the Radiographers which are using it.

4.4.3 Model-based prototype analyses for radiological dashboards

To narrow down the choice of KPIs is the main part of dashboard development. Within this scope, Karami et al. [33] have grouped nominal classes for radiological dashboards. The applicable group for the current work is "patient safety" in the field of "protocol selection error rate." The used KPI metric for the current dashboard mock-up is the local Weber contrast.

A full dashboard assessment based on the table "A Comprehensive Model for Designing Radiology Dashboard" prepared by Karami et al. [33] was performed. Similar to Chapter 4.4.1, the gray text lines are the statements from the scientific literature. Directly below, the mock-up analysis has been described.

a) *Determining the goal of dashboards to achieve the defined goals and how to calculate them*

   The goal of the dashboard is to visualize local contrast behaviors in digital plane radiographs; it refers to the research question in this thesis.

b) *Design of dashboards aligning with organizational goals and objectives*

The dashboard underlies no organizational goals and objectives. It was designed for scientific work as a mock-up prototype.

c) *Determine indicators that are critical and special in terms of the quality of their performance along with their calculation method and threshold*

Stable metrics ensured valid local contrast steps within the radiographs. This was empirically evaluated in the pretest phase (Chapter 4.1) in this thesis.

d) *Set the time interval for updating information based on the user's view, type of use, and importance of task*

The data capture has to be done once for each desired acquisition parameter to picture the local contrast behavior. The data is valid for the radiological image processing. To compare it with other detector systems and acquisition setups, the view is standardized and predefined.

e) *Extract accurate and relevant data with acceptable and standard definitions for calculation*

The used local Weber contrast is recommended by the IAEA and part of the image quality measurement methods. Their diagnostic radiology physics document [6] is widely accepted. As a data source, raw 16bit gray-scale DICOM files were used.

f) *Capability of optimizing, customization based on the requirement of users, organization, and changing circumstances*

The optimization process—in other words, the parameter adaptation—was realized as pseudo color tables over the total range of kV and mAs for different density steps. Within this scope, the user can adapt the acquisition parameter to optimize the local contrast for the needed density step. No customization has been implemented in the current dashboard mock-up. By changing the detector system or other relevant system components, the imaging process and the contrast feature calculation have to be performed again.

g) *The user's ability to perform an in-depth analysis by clicking on the operational indicators*

There is no possibility for the user to analyze the dashboard data by a click. Thus, the dashboard is realized as a mock-up within a specific use case.

h) *Procedures, techniques, and technologies used to protect data*

No patient information was needed to create the dashboard. The raw data taken from the radiograph includes the name of the institute, the detector system, the name of image processing workstation, and the X-ray system.

i) *Consider components of visual design, structure, layout, and presentation of information*

The visual design was executed in simplified terms. Regarding the layout and structure, a dashboard header, a supportive information field, and the main contrast area were created. The essential local contrast information is coded into false colors and presented as tables.

j) *A mechanism to highlight important information, such as exceptions, and outliers*

The local contrast information for each acquisition parameter was arranged into a table and coded with false colors. Three color classes were created to divide high, medium, and low contrast. The medium contrast class represents the $Q_{0,5}$ quantile within the table. No outliers were considered.

5 Discussion

All partial results are shown in the following paragraphs. Summarized, the dashboard development could be realized successfully for the chosen contrast metric. The image quality visualization is done in false color tables. Furthermore, a simple structured dashboard design was executed. The expert feedback indicates a higher job performance for radiographers. No misleading interpretation or patient risk is identified because of the professional competences of the target user group. If the knowledge from the user group is available the image quality would increase. According to that, the availability of the dashboard in a radiological department is a core element for image quality assessment in the radiographer's work.

The acquired image cluster represented all possible kV and mAs combinations over the X-ray generator—this implies that 84 radiographs with 12 different kV steps from 57kV to 109kV and seven different mAs steps from 10mAs to 40mAs were acquired.

The range of the validity of the raw metrics was investigated by performing a pre-test. This pre-test phase indicates the thickness of the permeated material and a lower confidence in the measured ROIs. In this case, the data reliability in a material of lower thickness is higher than that in thicker objects. The local contrast calculation was directly based on gray values and depends directly on such stable data. The measured data showed sufficient metrics for all the used features. During the pre-test phase, the variations expressed as standard deviation and standard error are stable for all extracted ROIs within the features. Within a kV domain, the data tables illustrate stable mean values. In further consideration, at low-intensity features (for example, Intensity Step 7) lower standard deviation and SEM results were identified in comparison with higher areas. The main influence factor is the kV. The higher the chosen kV, the higher the photon energy and the lower the absorption within the feature.

The feature extraction and the local contrast calculation were performed semi-manually with ImageJ 1.50f and Excel 2010. The two software products are suitable for attaining one's objects. An ROI set was defined to extract the raw values from the radiographs in a standardized structured way. The result tables contained mean, standard deviation, and minimum and maximum gray values. The intermediate result tables were exported as comma-separated files. The final local contrast calculation was performed with Excel. The numeric results confirm the physics-related principles and laws and are coherent to the pre-test results. The metric measurements within all features showed different data. These ensured an admissible basis to calculate the local contrast based on the extracted metrics. In more detailed analyses, the standard deviation and mean gray values are decreased when the kV is increased. The connectivity between a lower standard deviation and a higher kV is well founded in physics. The indirect link between kV and mean gray values is obvious. The plausible reasoning is that a radiograph happens to be a negative image: It is as higher as the measured signal on the detector and as lower as the encoded gray value.

The image quality visualization dashboard was realized as a mock-up. It was made up in three main areas and consists of supportive elements and local contrast tables. The visualization work task was performed with the software yEd, Excel, and Microsoft PowerPoint Professional Plus 2010. The needed additional information elements were designed, developed, and placed to read the dashboard and to provide a better understanding.

The main information are six color tables representing the contrast behavior for any local contrast from the radiographs. Each of these tables was arranged as a cluster with the kV in columns and mAs in rows. The color code setting was done with the web-based software ColorBrewer. Hence, print safe and color blind RGB classes were defined. A linear scale for the color grading was created. The highest contrast was fixed first class, while the lowest local contrast was fixed on the third class. For the second color class, the $Q_{0,5}$ quantile was calculated. A linear calculation was performed between these classes.

The dashboard analysis and evaluation was divided into three different steps. An empirical determination by two experts was performed. The image quality assessment and prototype analysis were performed based on the published scientific background.

Five open questions were formed based on the usefulness of the image quality dashboard and connected with the published scientific work. The feedback from the experts indicates higher image quality and job performance under certain circumstances. All necessary information for the image quality assessment are provided from to dashboard prototype. The main focus for the user group is supposed to the theoretical dashboard explanation and additional supportive information.

The image quality dashboard fulfilled the core statement “availability” for image quality improvement and analysis. Moreover, the development of key elements to secure acquisition protocols, picture an initial situation for data processing to ensure higher quality, and minimize poor X-ray image quality is supported by the dashboard. The image quality dashboard might be an important part of a clinical quality development process for radiographers.

A model-based analysis was applied to the image quality dashboard. This structured comprehensive view on the mock-up allows an overview of the defined goals, aligned objectives, and the ability to perform in-depth analysis. As it turns out, the Weber contrast was identified as the KPI and an accurate and relevant data metric. However, several issues remain open. Data optimization and user-based customization are not implemented in the current dashboard mock-up. Important information was not highlighted, and an elaborate design was not developed. The procedures and techniques to protect the data were not relevant in terms of the visualized information.

5.1 Dashboard limitations

Image quality assessment is only valid for the features within the test pattern. The test arrangement considers only one type of material density, which is equal to soft tissues in the human body. On the other hand, the local contrast is restricted to objects with a thickness of $1cm$. This corresponds roughly to digits or metacarpal bones rather than to all different body parts.

5.2 Further investigation

A contrast comparison could be realized as an interactive dashboard feature. By highlighting equal acquisition parameters in each table, a visual alignment for all contrast steps could be helpful.

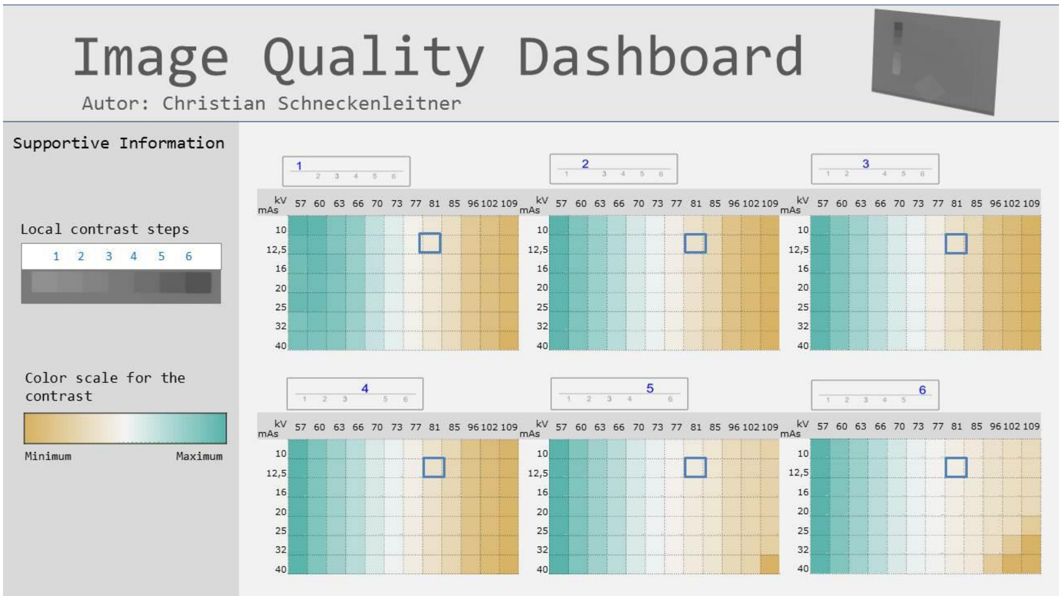

Figure 30. Interaction tool for better contrast comparison

In Figure 30, the blue fields mark the local contrast for all 81kV and 12.5mAs radiographs. This method can help identify conflicts of interest. Further developing and testing phases are capable of determining the over value for this software feature.

Moreover, a zoom could be realized for each local contrast field. This tool could allow a closer look at more detailed image quality metrics. A direct comparison of the two selected radiographs is shown in Figure 31.

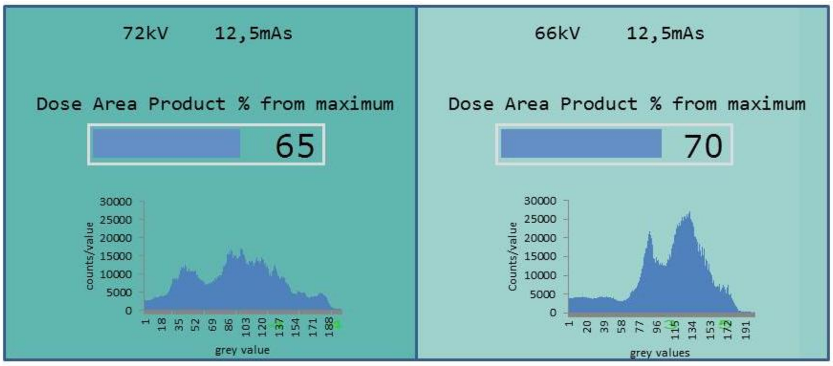

Figure 31. Additional visualization zoom elements for direct image comparison

The backgrounds of both boxes correspond to the color gradient from the image tables. The dose area product calculated from the DICOM header and a computed histogram are visualized.

6 Conclusion

Performing high-quality radiographs is the main focus for radiographers. The current image quality dashboard based on local contrast behaviors is a valid method to picture image quality to this occupational group. Digital X-rays are gray-scale intensity images, and the Weber contrast is an accurate image quality metric to evaluate the local contrast in these radiographs. After a comprehensive analysis and expert determination, the dashboard fulfills various criteria to ensure higher image quality and avoid poor X-ray acquisition parameters. Therefore, the availability of the dashboard in a radiology department is a core element for image quality assessment in the radiographer's work.

Modern DR detector systems are eminently suitable for producing the image cluster under laboratory considerations. The test pattern and the detector panel must not be replaced during the whole acquisition process. The detector functional principles were based on a wireless system, which is why this approach is applicable for future uses. A new study setup has to be established for CR detector systems.

The calculation based on gray values is trustworthy and can be carried out for image quantitative–image quality determination. The raw data exploration and parameters validation were essential for target-aimed visualization. Otherwise, a correct visualization could lead to a deceptive interpretation of local contrast behaviors in radiographs.

The image processing and analysis pipeline was prepared in a semi-automatic manner with different software solutions. To establish a more reliable image quality toolkit, a fully automated solution has to be developed. This allows a lower threshold for using the dashboard for a wider user group.

In the current state of research, the dashboard mock-up provides all the needed information to determine the local contrast behavior for an X-ray-based detector system. This was sufficient to perform the expert determination to investigate the usefulness of the image quality dashboard. No interaction is realized within the current scope. Next, the implementation of selective zoom elements and more detailed views of data could lead to a deeper understanding for the user.

For the future, the image quality toolkit, namely the dashboard, could be used to compare different detector systems and the expected local contrast behavior under certain acquisition parameters.

Literature

[1] M. Zimmer-Brossy, *Lehrbuch der röntgendiagnostischen Einstelltechnik: Begründet von Marianne Zimmer-Brossy*, 5th ed. Berlin: Springer, 1997.

[2] P. K. J. Dreyer, M. D. S. Hirschorn, M. J. H. Thrall, and M. A. Mehta, *PACS: A Guide to the Digital Revolution*, Softcover reprint of hardcover 2nd ed. 2006. New York: Springer, 2009.

[3] K. C. Wang, R. W. Filice, J. F. Philbin, E. L. Siegel, and P. G. Nagy, “Five levels of PACS modularity: integrating 3D and other advanced visualization tools,” *J Digit Imaging*, vol. 24, no. 6, pp. 1096–1102, Dec. 2011.

[4] H. Morneburg, *Bildgebende Systeme für die medizinische Diagnostik: Röntgendiagnostik und Angiographie/ Computertomographie/ Nuklearmedizin/ Magnetresonanztomographie/ Sonographie/ Integrierte Informationssysteme*, 3rd ed. Erlangen: Publicis Publishing, 1995.

[5] L. Lanca and A. Silva, *Digital Imaging Systems for Plain Radiography*. New York, NY: Springer, 2013.

[6] IAEA, “Diagnostic Radiology Physics,” 2014.

[7] A. Frößler, *Konventionelle Röntgendiagnostik: Einstelltechnik und Röntgenanatomie*. München: Elsevier, 2005.

[8] K. J. Strauss and S. C. Kaste, “The ALARA (as low as reasonably achievable) concept in pediatric interventional and fluoroscopic imaging: striving to keep radiation doses as low as possible during fluoroscopy of pediatric patients—a white paper executive summary,” *Pediatr Radiol*, vol. 36, no. Suppl 2, pp. 110–112, Sep. 2006.

[9] W. Birkfellner, *Applied Medical Image Processing: A Basic Course*. Boca Raton: Taylor & Francis, 2010.

[10] H. Krieger, *Grundlagen der Strahlungsphysik und des Strahlenschutzes*, 3rd ed. Wiesbaden: Vieweg+Teubner Verlag, 2009.

[11] M. Uffmann *et al.*, “Flat-panel-detector chest radiography: effect of tube voltage on image quality,” *Radiology*, vol. 235, no. 2, pp. 642–650, May 2005.

[12] K. Tang, L. Wang, R. Li, J. Lin, X. Zheng, and G. Cao, “Effect of Low Tube Voltage on Image Quality, Radiation Dose, and Low-Contrast Detectability at Abdominal Multidetector CT: Phantom Study,” *BioMed Research International*, vol. 2012, p. e130169, Apr. 2012.

[13] M. Sonoda, M. Takano, J. Miyahara, and H. Kato, “Computed radiography utilizing scanning laser stimulated luminescence.,” *Radiology*, vol. 148, no. 3, pp. 833–838, Sep. 1983.

[14] E. Kotter and M. Langer, “Digital radiography with large-area flat-panel detectors,” *Eur Radiol*, vol. 12, no. 10, pp. 2562–2570, Oct. 2002.

[15] R. Fasbender and R. Schaetzing, “Neue CR-Technologien für die digitale Radiographie,” *Radiologe*, vol. 43, no. 5, pp. 367–373, May 2003.

[16] M. B. Williams *et al.*, “Digital Radiography Image Quality: Image Acquisition,” *Journal of the American College of Radiology*, vol. 4, no. 6, pp. 371–388, Jun. 2007.

[17] H. H. Barrett, “Objective assessment of image quality: effects of quantum noise and object variability,” *J. Opt. Soc. Am. A, JOSAA*, vol. 7, no. 7, pp. 1266–1278, Jul. 1990.

[18] H. Handels, *Medizinische Bildverarbeitung: Bildanalyse, Mustererkennung und Visualisierung für die computergestützte ärztliche Diagnostik und Therapie*, 2nd ed. Wiesbaden: Vieweg+Teubner Verlag, 2009.
[19] A. R. Cowen, A. G. Davies, and S. M. Kengyelics, “Advances in computed radiography systems and their physical imaging characteristics,” *Clinical Radiology*, vol. 62, no. 12, pp. 1132–1141, Dezember 2007.
[20] “PS3.1.” [Online]. Available: http://dicom.nema.org/medical/dicom/current/output/html/part01.html. [Accessed: 17-Jun-2017].
[21] “PS3.5.” [Online]. Available: http://dicom.nema.org/medical/dicom/current/output/chtml/part05/PS3.5.html. [Accessed: 17-Jun-2017].
[22] “PS3.6.” [Online]. Available: http://dicom.nema.org/medical/dicom/current/output/html/part06.html. [Accessed: 17-Jun-2017].
[23] “6 DICOM Information Model.” [Online]. Available: http://dicom.nema.org/medical/dicom/current/output/chtml/part03/chapter_6.html. [Accessed: 17-Jun-2017].
[24] *Digital Image Processing - An Algorithmic Introduction Using | Wilhelm Burger | Springer*. .
[25] T. Munzner, *Visualization Analysis and Design: Principles, Techniques, and Practice*. Boca Raton: AK Peters Visualization Series, 2014.
[26] “Healthcare data analysis and visualization,” *Tableau Software*. [Online]. Available: https://www.tableau.com/solutions/topic/healthcare. [Accessed: 04-Jul-2017].
[27] J. D. C. Little, “Models and Managers: The Concept of a Decision Calculus,” *Management Science*, vol. 50, no. 12_supplement, pp. 1841–1853, Dec. 2004.
[28] D. Dowding *et al.*, “Dashboards for improving patient care: review of the literature,” *Int J Med Inform*, vol. 84, no. 2, pp. 87–100, Feb. 2015.
[29] “QIPP Urgent Care Clinical Dashboard — NHS Networks.” [Online]. Available: https://www.networks.nhs.uk/nhs-networks/qipp-urgent-care-gp-dashboard. [Accessed: 06-Jul-2017].
[30] J. A. Linder *et al.*, “Electronic health record feedback to improve antibiotic prescribing for acute respiratory infections,” *Am J Manag Care*, vol. 16, no. 12 Suppl HIT, pp. e311-319, Dec. 2010.
[31] M. B. Morgan, B. F. Branstetter, D. M. Lionetti, J. S. Richardson, and P. J. Chang, “The Radiology Digital Dashboard: Effects on Report Turnaround Time,” *J Digit Imaging*, vol. 21, no. 1, pp. 50–58, Mar. 2008.
[32] M. Karami, R. Safdari, and A. Rahimi, “Effective radiology dashboards: key research findings,” *Radiol Manage*, vol. 35, no. 2, pp. 42–45, Apr. 2013.
[33] M. Karami, “A Design Protocol to Develop Radiology Dashboards,” *Acta Inform Med*, vol. 22, no. 5, pp. 341–346, Oct. 2014.
[34] “ColorBrewer: Color Advice for Maps.” [Online]. Available: http://colorbrewer2.org/#type=sequential&scheme=BuGn&n=3. [Accessed: 16-Jun-2017].

List of Figures

List of Tables

Appendix

A.DICOM Image Header Information

0002,0002 Media Storage SOP Class UID: 1.2.840.10008.5.1.4.1.1.1.1

0002,0003 Media Storage SOP Inst UID: 1.3.46.670589.30.34.2.1.1625493452.1480498587708.2

0002,0010 Transfer Syntax UID: 1.2.840.10008.1.2.1

0002,0012 Implementation Class UID: 1.3.12.2.1107.5.99.3.20080101

0002,0013 Implementation Version Name: SIEMENS

0008,0005 Specific Character Set: ISO_IR 100

0008,0008 Image Type: ORIGINAL\PRIMARY\

0008,0016 SOP Class UID: 1.2.840.10008.5.1.4.1.1.1.1

0008,0018 SOP Instance UID: 1.3.46.670589.30.34.2.1.1625493452.1480498587708.2

0008,0020 Study Date: 20161130

0008,0021 Series Date: 20161130

0008,0022 Acquisition Date: 20161130

0008,0023 Image Date: 20161130

0008,0030 Study Time: 103432

0008,0031 Series Time: 103435

0008,0032 Acquisition Time: 103435

0008,0033 Image Time: 103435

0008,0050 Accession Number:

0008,0060 Modality: DX

0008,0068 Presentation Intent Type: FOR PRESENTATION

0008,0070 Manufacturer: Philips Medical Systems

0008,0080 Institution Name: FH Campus Wien

0008,0081 Institution Address: Initial Street Name Initial City Name Initial Country Name

0008,0090 Referring Physician's Name: ^^^^=^^^^=^^^^

0008,1010 Station Name: PDREleva01

0008,1030 Study Description: Schädel ohne Processing

0008,103E Series Description: Schädel ohne Processing

0008,1040 Institutional Department Name: Röntgen

0008,1050 Attending Physician's Name:

0008,1060 Name of Physician(s) Reading Study: ^^^^=^^^^=^^^^

0008,1070 Operator's Name: eleva

0008,1090 Manufacturer's Model Name: ProGrade

0008,1111 Referenced Study Component Sequence:

0008,1150 Referenced SOP Class UID: 1.2.840.10008.3.1.2.3.3

0008,1155 Referenced SOP Instance UID: 1.3.46.670589.30.34.2.1.1625493452.1480498336201.1

0008,2111 Derivation Description: Compress JPEG Lossless,Patient Name Corrected SHS, Decompress Pegasus JPEG Lossless

0008,3010 ---: 1.3.46.670589.30.34.2.1.1625493452.1480498472753.1

0010,0010 Patient's Name: Schneckenleitner^57

0010,0020 Patient ID: 20161130-01-0001

0010,0021 Issuer of Patient ID:

0010,0030 Patient's Birth Date:

0010,0040 Patient's Sex: O

0010,1000 Other Patient IDs:

0010,1010 Patient's Age:

0010,1020 Patient's Size: 0

0010,1030 Patient's Weight: 0

0010,21B0 Additional Patient History:

0010,21C0 ---: 4

0010,4000 Patient Comments:

0018,0015 Body Part Examined: SKULL

0018,0060 kVp: 57

0018,1000 Device Serial Number: 1625493452

0018,1020 Software Versions(s): 1.1.1

0018,1030 Protocol Name: Schädel ohne Processing

0018,1050 Spatial Resolution: 0.148

0018,1150 Exposure Time: 41

0018,1152 Exposure: 25

0018,1153 Exposure in uAs: 25000

0018,115E Image Area Dose Product: 3.597

0018,1164 Imager Pixel Spacing: 0.148\0.148

0018,1400 Acquisition Device Processing Description: C/B:32767.0/16383.5

0018,1405 Relative X-ray Exposure: 51

0018,1508 Positioner Type: NONE

0018,1600 Shutter Shape: POLYGONAL

0018,1620 Vertices of the Polygonal Shutter: 0\0\0\1887\1498\1887\1498\0

0018,1700 Collimator Shape: RECTANGULAR

0018,1702 Collimator Left Vertical Edge: 0

0018,1704 Collimator Right Vertical Edge: 1887

0018,1706 Collimator Upper Horizontal Edge: 0

0018,1708 Collimator Lower Horizontal Edge: 1498

0018,5101 View Position: AP

0018,7001 Detector Temperature: 34.6

0018,7004 Detector Type: SCINTILLATOR

0018,7008 Detector Mode: SingleShot1s

0018,700A Detector ID: SN143178

0018,700C Date of Last Detector Calibration: 20160616

0018,700E Time of Last Detector Calibration: 104310

0018,7012 Detector Time Since Last Exposure: 14600.618

0018,702A ---: TRIXELL

0018,702B ---: PIXIUM2430EZ

0018,7030 Field of View Origin: 0\0

0018,7032 Field of View Rotation: 0

0018,7034 Field of View Horizontal Flip: NO

0018,8150 ---: 40700

0020,000D Study Instance UID: 1.3.46.670589.30.34.2.1.1625493452.1480498333892.1

0020,000E Series Instance UID: 1.3.46.670589.30.34.2.1.1625493452.1480498589641.1

0020,0010 Study ID: S-IW4QHDJ8.1

0020,0011 Series Number: 1

0020,0013 Image Number: 1

0020,0020 Patient Orientation: \

0020,0052 Frame of Reference UID: 1.3.46.670589.30.34.2.1.1625493452.1480498589647.2

0020,1040 Position Reference Indicator:

0028,0002 Samples per Pixel: 1

0028,0004 Photometric Interpretation: MONOCHROME2

0028,0010 Rows: 1499

0028,0011 Columns: 1888

0028,0100 Bits Allocated: 16

0028,0101 Bits Stored: 15

0028,0102 High Bit: 14

0028,0103 Pixel Representation: 0

0028,0300 Quality Control Image: NO

0028,0301 Burned In Annotation: NO

0028,1040 Pixel Intensity Relationship: LOG

0028,1041 Pixel Intensity Relationship Sign:

0028,1050 Window Center: 16383

0028,1051 Window Width: 32767

0028,1052 Rescale Intercept: 0

0028,1053 Rescale Slope: 1

0028,1054 Rescale Type: US

0028,2110 Lossy Image Compression: 00

0032,1030 Reason for Study:

0032,1032 Requesting Physician: ^^^^=^^^^=^^^^

0032,1033 Requesting Service:

0032,1060 Requested Procedure Description:

0032,4000 Study Comments:

0040,0241 Performed Station AE Title: PDRWS1

0040,0244 Performed Procedure Step Start Date: 20161130

0040,0245 Performed Procedure Step Start Time: 103432.830000

0040,0250 Performed Procedure Step End Date: 20161130

0040,0251 Performed Procedure Step End Time: 103627.540000

0040,0252 Performed Procedure Step Status: IN PROGRESS

0040,0253 Performed Procedure Step ID: E-IW4QHFBA.1

0040,0254 Performed Procedure Step Description: Schädel ohne Processing

0040,0260 Performed Action Item Sequence:

0008,0100 Code Value: RO.RO0601

0008,0102 Coding Scheme Designator:

0008,0104 Code Meaning:
0040,0275 Request Attributes Sequence:
0040,0009 Scheduled Procedure Step ID:
0040,1001 Requested Procedure ID:
0040,0301 Total Number of Exposures: 1
0040,0302 Entrance Dose: 0
0040,0320 Billing Procedure Step Sequence:
0040,0321 Film Consumption Sequence:
0040,0555 Acquisition Context Sequence:
0040,1001 Requested Procedure ID:
0040,1002 Reason for the Requested Procedure:
0040,1003 Requested Procedure Priority:
0040,1004 Patient Transport Arrangements:
0040,1010 Names of Intended Recipients of Results:
0040,1400 Requested Procedure Comments:
0040,2001 Reason for the Imaging Service Request:
0040,2004 Issue Date of Imaging Service Request:
0040,2400 Imaging Service Request Comments:
0040,8302 Entrance Dose in mGy: 0
0095,0010 ---: SIENET
0095,10FA ---: ^^^^=^^^^=^^^^
2001,0010 ---: Philips Imaging DD 001
2001,0011 ---: Philips Imaging DD 002
2001,0090 ---: Philips Imaging DD 129
2001,1063 ---: ELSEWHERE
2001,10C1 ---: GraphicOverlayPlane
2001,116C ---: E-IW4QHFBA.1
200B,0010 ---: Philips RAD Imaging DD 001
200B,0070 ---: Philips RAD Imaging DD 097
200B,0072 ---: Philips RAD Imaging DD 099
200B,1001 ---: 4
200B,1002 ---: 7
200B,1005 ---: 2
200B,1011 ---: Schädel ap
200B,1027 ---: 30000101000000.000000
200B,1028 ---: 3.597
200B,1029 ---: 0
200B,102B ---: 20161130
200B,102C ---: 103216
200B,102E ---: 410
200B,103B ---: Schädel ohne Processing
200B,1041 ---: TRUE
200B,1042 ---: 1.3.46.670589.30.34.2.1.1625493452.1480498336201.1
200B,1047 ---: 20161130
200B,1048 ---: FALSE
200B,104C ---: COMPLETED
200B,104F ---: 20161130103435.278000

200B,1052 ---: NORMAL
200B,7000 ---: file:/G:/Images/gxrFH_C3349665150141709164.gip
200B,7060 ---: ACQUISITION_5350_4297
200B,7063 ---: C/B:32767.0/16383.5
200B,7074 ---: 13
200B,7076 ---: standard
200B,7079 ---: 6000
200B,707A ---: 5
200B,707E ---: 1.3.46.670589.30.34.2.1.1625493452.1480498589879.1
200B,7088 ---: TRUE
200B,7089 ---: DXIMAGE_1057_885
200B,7096 ---: Portable
200B,70A5 ---: 27.6
200B,70B7 ---: 0
200B,70B9 ---: TRUE
200B,70BA ---: LARGE
200B,7235 ---: 0
2050,0020 ---: IDENTITY
6000,0010 ---: 1499
6000,0011 ---: 1888
6000,0040 ---: G
6000,0100 ---: 1
6000,0102 ---: 0
7FE0,0010 Pixel Data: 359844

B Image cluster raw data. Minimum, maximum and mean grey value

Min value	Max value	Mean value	Image
0	11832	7880.291	1
0	12394	8492.946	2
0	13037	9110.205	3
0	13596	9670.855	4
0	14179	10232.944	5
0	14844	10861.738	6
0	15445	11435.584	7
0	12583	8639.792	8
0	13167	9195.755	9
0	13791	9815.165	10
0	14360	10376.362	11
0	14984	10942.992	12
0	15615	11571.010	13
0	16206	12150.366	14
0	13334	9344.857	15
0	13887	9902.598	16
0	14588	10525.600	17
0	15204	11095.293	18
0	15727	11654.941	19
0	16429	12291.891	20
0	16965	12859.425	21
0	15185	10993.896	22
0	15761	11552.800	23
0	16430	12175.442	24
0	17033	12741.051	25
0	17597	13308.176	26
0	18251	13942.041	27
0	18828	14523.133	28
0	15990	11742.535	29
0	16580	12304.415	30
0	17285	12928.659	31
0	17757	13495.910	32
0	18383	14069.553	33
0	19055	14705.483	34
0	19594	15280.201	35
0	16920	12588.300	36
8942	17518	13377.937	37
0	18181	13776.870	38
10140	18763	14592.947	39
0	19324	14919.275	40
0	19990	15555.933	41
0	20665	16137.448	42

Min value	Max value	Mean value	Image
8967	18026	13803.786	43
0	18628	14131.013	44
10150	19221	15011.604	45
0	19888	15330.095	46
11294	20504	16175.625	47
11924	21153	16818.702	48
0	21782	17105.656	49
0	18984	14396.674	50
0	19573	14962.010	51
10628	20214	15859.899	52
11196	20810	16436.006	53
11748	21465	17008.426	54
12385	22198	17646.807	55
0	22848	17919.182	56
0	20389	15613.921	57
0	21052	16175.424	58
0	21692	16799.565	59
0	22220	17364.409	60
0	22805	17933.100	61
0	23411	18551.436	62
0	24167	19129.556	63
0	21637	16638.849	64
0	22028	17194.216	65
0	22862	17817.290	66
0	23555	18383.280	67
0	24053	18952.824	68
0	24807	19585.893	69
0	25502	20167.876	70
0	22833	17803.014	71
0	23521	18373.536	72
0	24155	18998.195	73
0	25044	19564.699	74
0	25563	20131.822	75
0	26347	20762.138	76
0	27115	21335.377	77
0	24597	19180.119	78
0	25290	19740.961	79
0	26083	20360.999	80
0	26944	20943.976	81
0	27889	21514.559	82
0	29722	22150.421	83
0	30412	22705.350	84

C Calculated mean and standard deviation inform all features (ROI) and the whole image content (All)

Label	Slice	Mean ROI	Mean All	StdDev ROI	StdDev All
Stack:5710000	1	22341	22705	3999	3174
Stack:5712500	2	21752	22150	3987	3050
Stack:5716000	3	21102	21515	3979	2971
Stack:5720000	4	20518	20944	3974	2900
Stack:5725000	5	19944	20361	3976	2877
Stack:5732000	6	19311	19741	3968	2799
Stack:5740000	7	18742	19180	3968	2729
Stack:6010000	8	20996	21335	3612	2921
Stack:6012500	9	20417	20762	3614	2850
Stack:6016000	10	19771	20132	3611	2772
Stack:6020000	11	19198	19565	3611	2702
Stack:6025000	12	18623	18998	3609	2632
Stack:6032000	13	17985	18374	3602	2555
Stack:6040000	14	17420	17803	3600	2527
Stack:6310000	15	19871	20168	3307	2755
Stack:6312500	16	19280	19586	3304	2682
Stack:6316000	17	18634	18953	3300	2604
Stack:6320000	18	18056	18383	3301	2534
Stack:6325000	19	17480	17817	3297	2464
Stack:6332000	20	16846	17194	3294	2387
Stack:6340000	21	16279	16639	3292	2320
Stack:6610000	22	18857	19130	3036	2609
Stack:6612500	23	18270	18551	3035	2537
Stack:6616000	24	17636	17933	3031	2461
Stack:6620000	25	17057	17364	3030	2391
Stack:6625000	26	16484	16800	3029	2321
Stack:6632000	27	15847	16175	3024	2245
Stack:6640000	28	15277	15614	3022	2176
Stack:7010000	29	17671	17919	2730	2441
Stack:7012500	30	17081	17647	2722	719
Stack:7016000	31	16443	17008	2721	719
Stack:7020000	32	15869	16436	2719	719
Stack:7025000	33	15295	15860	2717	718
Stack:7032000	34	14665	14962	2720	2075
Stack:7040000	35	14093	14397	2715	2006
Stack:7310000	36	16880	17106	2537	2327
Stack:7312500	37	16291	16819	2530	679
Stack:7316000	38	15649	16176	2528	678
Stack:7320000	39	15075	15330	2531	2107
Stack:7325000	40	14490	15012	2521	677
Stack:7332000	41	13864	14131	2523	1959
Stack:7340000	42	13286	13804	2514	675
Stack:7710000	43	15943	16137	2323	2193
Stack:7712500	44	15352	15556	2321	2121
Stack:7716000	45	14708	14919	2317	2042
Stack:7720000	46	14120	14593	2309	632
Stack:7725000	47	13554	13777	2310	1900
Stack:7732000	48	12909	13378	2301	628

Stack:7740000	49	12343	12588	2301	1754
Stack:8110000	50	15110	15280	2146	2076
Stack:8112500	51	14530	14705	2144	2005
Stack:8116000	52	13887	14070	2141	1926
Stack:8120000	53	13304	13496	2137	1854
Stack:8125000	54	12727	12929	2132	1784
Stack:8132000	55	12091	12304	2126	1707
Stack:8140000	56	11519	11743	2121	1638
Stack:8510000	57	14386	14523	1998	2008
Stack:8512500	58	13795	13942	1994	1935
Stack:8516000	59	13152	13308	1991	1854
Stack:8520000	60	12574	12741	1986	1782
Stack:8525000	61	11997	12175	1982	1710
Stack:8532000	62	11362	11553	1976	1632
Stack:8540000	63	10796	10994	1970	1562
Stack:9610000	64	12755	12859	1696	1809
Stack:9612500	65	12173	12292	1691	1707
Stack:9616000	66	11527	11655	1688	1653
Stack:9620000	67	10956	11095	1684	1555
Stack:9625000	68	10378	10526	1679	1508
Stack:9632000	69	9747	9903	1672	1428
Stack:9640000	70	9242	9345	1564	1351
Stack:10210000	71	12054	12150	1576	1711
Stack:10212500	72	11473	11571	1574	1662
Stack:10216000	73	10832	10943	1570	1579
Stack:10220000	74	10256	10376	1566	1505
Stack:10225000	75	9686	9815	1560	1431
Stack:10232000	76	9111	9196	1464	1345
Stack:10240000	77	8619	8640	1351	1267
Stack:10910000	78	11353	11436	1468	1640
Stack:10912500	79	10769	10862	1465	1564
Stack:10916000	80	10130	10233	1460	1480
Stack:10920000	81	9559	9671	1455	1407
Stack:10925000	82	9029	9110	1381	1330
Stack:10932000	83	8484	8493	1253	1243
Stack:10940000	84	8093	7880	1065	1357

D Reliability testing for the feature metric with mean, standard deviation and standard error of the mean

Label	Mean	StdDev	Min	Max	Slice	SE	SEM
ROI1:4810001	31124	1318	27940	32767	1	498,16	
ROI1:4810002	31303	1294	27650	32767	2	489,09	
ROI1:4810003	31256	1312	27877	32767	3	495,89	
ROI1:4810004	31249	1304	27743	32767	4	492,87	491,73
ROI1:4810005	31283	1297	27889	32767	5	490,22	
ROI1:4810006	31275	1302	27877	32767	6	492,11	
ROI1:4810008	31335	1280	28044	32767	7	483,79	
ROI1:7725001	14664	42	14518	14802	8	15,87	
ROI1:7725002	14660	42	14515	14793	9	15,87	
ROI1:7725003	14661	42	14493	14783	10	15,87	
ROI1:7725004	14660	42	14487	14783	11	15,87	15,82
ROI1:7725005	14663	41	14489	14796	12	15,50	
ROI1:7725006	14660	42	14504	14799	13	15,87	
ROI1:7725007	14660	42	14508	14776	14	15,87	
ROI2:4810001	30680	1340	27517	32767	1	506,47	
ROI2:4810002	30914	1340	27593	32767	2	506,47	
ROI2:4810003	30814	1341	27685	32767	3	506,85	
ROI2:4810004	30830	1347	27605	32767	4	509,12	506,36
ROI2:4810005	30915	1336	27462	32767	5	504,96	
ROI2:4810006	30949	1340	27474	32767	6	506,47	
ROI2:4810008	30934	1334	27877	32767	7	504,20	
ROI2:7725001	13938	39	13790	14067	8	14,74	
ROI2:7725002	13935	39	13795	14087	9	14,74	
ROI2:7725003	13935	39	13787	14043	10	14,74	
ROI2:7725004	13934	38	13802	14045	11	14,36	14,63
ROI2:7725005	13935	39	13785	14071	12	14,74	
ROI2:7725006	13933	38	13790	14047	13	14,36	
ROI2:7725007	13933	39	13781	14046	14	14,74	
ROI3:4810001	28883	935	26735	32767	1	353,40	
ROI3:4810002	29062	997	26900	32767	2	376,83	
ROI3:4810003	29014	975	26900	32767	3	368,52	
ROI3:4810004	29008	985	26800	32767	4	372,30	371,65
ROI3:4810005	29033	973	26703	32767	5	367,76	
ROI3:4810006	29094	1002	27005	32767	6	378,72	
ROI3:4810008	29105	1016	26703	32767	7	384,01	
ROI3:7725001	12897	33	12775	13003	8	12,47	
ROI3:7725002	12891	33	12783	12993	9	12,47	
ROI3:7725003	12891	33	12757	12990	10	12,47	
ROI3:7725004	12890	33	12762	12994	11	12,47	12,47
ROI3:7725005	12891	33	12768	13004	12	12,47	
ROI3:7725006	12888	33	12772	12999	13	12,47	
ROI3:7725007	12887	33	12769	12989	14	12,47	
ROI4:4810001	25822	314	24881	27390	1	118,68	
ROI4:4810002	25899	315	25010	27390	2	119,06	
ROI4:4810003	25894	316	24973	27087	3	119,44	
ROI4:4810004	25877	315	24913	27200	4	119,06	120,25
ROI4:4810005	25897	318	24865	27278	5	120,19	
ROI4:4810006	25915	326	24989	27390	6	123,22	
ROI4:4810008	25906	323	25010	27442	7	122,08	

ROI4:7725001	11675	24	11599	11753	8	9,07	
ROI4:7725002	11666	25	11588	11756	9	9,45	
ROI4:7725003	11666	24	11576	11739	10	9,07	
ROI4:7725004	11665	25	11591	11742	11	9,45	9,23
ROI4:7725005	11667	24	11586	11750	12	9,07	
ROI4:7725006	11663	25	11591	11748	13	9,45	
ROI4:7725007	11661	24	11593	11745	14	9,07	
ROI5:4810001	22679	150	22087	23204	1	56,69	
ROI5:4810002	22747	150	22237	23297	2	56,69	
ROI5:4810003	22740	151	22186	23375	3	57,07	
ROI5:4810004	22741	149	22159	23263	4	56,32	56,37
ROI5:4810005	22747	147	22192	23306	5	55,56	
ROI5:4810006	22758	148	22203	23297	6	55,94	
ROI5:4810008	22749	149	22243	23305	7	56,32	
ROI5:7725001	10431	31	10333	10519	8	11,72	
ROI5:7725002	10420	31	10327	10516	9	11,72	
ROI5:7725003	10418	31	10315	10513	10	11,72	
ROI5:7725004	10417	30	10326	10509	11	11,34	11,61
ROI5:7725005	10419	30	10329	10505	12	11,34	
ROI5:7725006	10414	31	10315	10503	13	11,72	
ROI5:7725007	10411	31	10318	10509	14	11,72	
ROI6:4810001	19008	82	18738	19296	1	30,99	
ROI6:4810002	19041	83	18757	19324	2	31,37	
ROI6:4810003	19035	80	18739	19294	3	30,24	
ROI6:4810004	19038	81	18702	19342	4	30,62	30,94
ROI6:4810005	19042	81	18775	19335	5	30,62	
ROI6:4810006	19050	82	18748	19327	6	30,99	
ROI6:4810008	19041	84	18726	19307	7	31,75	
ROI6:7725001	8873	26	8797	8954	8	9,83	
ROI6:7725002	8858	25	8775	8930	9	9,45	
ROI6:7725003	8854	25	8777	8930	10	9,45	
ROI6:7725004	8853	25	8780	8929	11	9,45	9,56
ROI6:7725005	8855	25	8783	8926	12	9,45	
ROI6:7725006	8848	26	8771	8919	13	9,83	
ROI6:7725007	8845	25	8767	8916	14	9,45	
ROI7:4810001	15078	31	14964	15204	1	11,72	
ROI7:4810002	15095	31	14977	15198	2	11,72	
ROI7:4810003	15093	31	14988	15208	3	11,72	
ROI7:4810004	15096	31	14990	15215	4	11,72	11,72
ROI7:4810005	15097	31	14985	15204	5	11,72	
ROI7:4810006	15100	31	14987	15214	6	11,72	
ROI7:4810008	15094	31	14987	15202	7	11,72	
ROI7:7725001	7118	17	7071	7177	8	6,43	
ROI7:7725002	7093	17	7041	7150	9	6,43	
ROI7:7725003	7086	17	7032	7144	10	6,43	
ROI7:7725004	7084	17	7029	7147	11	6,43	6,43
ROI7:7725005	7089	17	7041	7151	12	6,43	
ROI7:7725006	7077	17	7028	7137	13	6,43	
ROI7:7725007	7074	17	7020	7133	14	6,43	

E Local contrast metrics for 6 different steps

mAs	Label	Contrast 1	Contrast 2	Contrast 3	Contrast 4	Contrast 5	Contrast 6
10	ROI1:5710000	859	1670	2003	2198	2659	2477
12,5	ROI1:5712500	846	1657	2014	2197	2655	2481
16	ROI1:5716000	836	1655	2006	2200	2650	2486
20	ROI1:5720000	836	1648	1998	2192	2648	2486
25	ROI1:5725000	845	1653	2002	2193	2653	2482
32	ROI1:5732000	823	1648	1995	2197	2654	2476
40	ROI1:5740000	829	1643	1997	2196	2659	2468
10	ROI1:6010000	853	1526	1793	1970	2396	2267
12,5	ROI1:6012500	846	1526	1799	1971	2401	2266
16	ROI1:6016000	845	1527	1796	1969	2400	2269
20	ROI1:6020000	838	1535	1795	1971	2403	2265
25	ROI1:6025000	841	1524	1799	1970	2406	2257
32	ROI1:6032000	830	1522	1794	1969	2409	2249
40	ROI1:6040000	823	1520	1791	1970	2408	2245
10	ROI1:6310000	821	1414	1636	1788	2192	2091
12,5	ROI1:6312500	817	1422	1630	1784	2191	2090
16	ROI1:6316000	825	1412	1623	1785	2198	2079
20	ROI1:6320000	818	1412	1627	1788	2199	2074
25	ROI1:6325000	819	1406	1626	1784	2201	2067
32	ROI1:6332000	818	1406	1622	1786	2198	2066
40	ROI1:6340000	814	1406	1620	1792	2191	2063
10	ROI1:6610000	802	1309	1481	1630	2015	1934
12,5	ROI1:6612500	794	1312	1479	1628	2021	1926
16	ROI1:6616000	793	1305	1482	1630	2019	1914
20	ROI1:6620000	798	1305	1478	1630	2021	1909
25	ROI1:6625000	795	1300	1481	1634	2018	1907
32	ROI1:6632000	791	1302	1477	1637	2008	1907
40	ROI1:6640000	786	1299	1478	1638	2003	1906
10	ROI1:7010000	751	1186	1317	1454	1821	1746

12,5	ROI1:7012500	751	1183	1316	1454	1823	1737
16	ROI1:7016000	751	1180	1318	1457	1820	1734
20	ROI1:7020000	753	1176	1320	1461	1811	1733
25	ROI1:7025000	747	1178	1315	1466	1806	1731
32	ROI1:7032000	750	1179	1319	1459	1802	1731
40	ROI1:7040000	746	1176	1320	1452	1800	1729
10	ROI1:7310000	719	1103	1218	1345	1695	1625
12,5	ROI1:7312500	724	1100	1217	1348	1692	1620
16	ROI1:7316000	721	1099	1218	1353	1684	1619
20	ROI1:7320000	722	1097	1217	1354	1678	1616
25	ROI1:7325000	715	1099	1220	1347	1674	1615
32	ROI1:7332000	714	1101	1219	1341	1672	1615
40	ROI1:7340000	715	1103	1213	1338	1670	1614
10	ROI1:7710000	682	1013	1109	1231	1548	1490
12,5	ROI1:7712500	680	1013	1109	1233	1542	1487
16	ROI1:7716000	679	1013	1110	1231	1534	1487
20	ROI1:7720000	676	1015	1113	1224	1531	1485
25	ROI1:7725000	678	1018	1107	1219	1530	1484
32	ROI1:7732000	680	1015	1101	1217	1530	1483
40	ROI1:7740000	680	1009	1097	1217	1528	1480
10	ROI1:8110000	643	942	1020	1137	1424	1378
12,5	ROI1:8112500	644	941	1026	1132	1420	1378
16	ROI1:8116000	641	944	1024	1127	1417	1376
20	ROI1:8120000	643	946	1019	1123	1416	1376
25	ROI1:8125000	644	943	1014	1120	1414	1373
32	ROI1:8132000	642	936	1010	1119	1413	1371
40	ROI1:8140000	638	931	1008	1119	1412	1363
10	ROI1:8510000	611	878	954	1051	1324	1286
12,5	ROI1:8512500	608	882	951	1045	1321	1286
16	ROI1:8516000	611	883	945	1044	1320	1284
20	ROI1:8520000	609	880	940	1042	1320	1282
25	ROI1:8525000	608	873	939	1041	1318	1279

32	ROI1:8532000	604	870	935	1040	1316	1272
40	ROI1:8540000	601	867	934	1039	1313	1261
10	ROI1:9610000	535	755	794	884	1129	1097
12,5	ROI1:9612500	532	750	793	883	1128	1096
16	ROI1:9616000	528	747	791	883	1126	1093
20	ROI1:9620000	527	747	789	882	1124	1088
25	ROI1:9625000	524	746	788	879	1121	1076
32	ROI1:9632000	524	744	785	880	1113	1064
40	ROI1:9640000	524	742	784	877	1104	561
10	ROI1:10210000	498	706	732	822	1052	1020
12,5	ROI1:10212500	497	705	729	823	1050	1019
16	ROI1:10216000	494	703	730	820	1049	1014
20	ROI1:10220000	494	703	728	820	1045	1005
25	ROI1:10225000	495	700	727	818	1040	993
32	ROI1:10232000	493	700	725	815	1029	559
40	ROI1:10240000	493	697	723	809	1002	22
10	ROI1:10910000	466	665	674	765	981	951
12,5	ROI1:10912500	464	665	672	765	980	948
16	ROI1:10916000	464	663	670	764	977	937
20	ROI1:10920000	464	662	670	762	970	929
25	ROI1:10925000	463	660	669	759	960	602
32	ROI1:10932000	462	659	666	751	927	10
40	ROI1:10940000	443	654	665	741	389	0

D Expert questionary to evaluate the usefulness of the image quality dashboard

The title of the research work:

Visualization toolkit for image quality assessment in digital radiographs

Some Explanations

In the present case, a slide is realized as a prototype. This low executed mockup of an image quality dashboard should supports radiographer to estimate local contrast behavior in radiographs.

The following five questions are based on the technology acceptance model and framed to evaluate the appraisal usefulness. Please answer the following questions in a descriptive manner.

Thanks four support the development of this framework!

Questions to your person:

a. Do you have work experience in a university filed? (Yes/No)

b. How long is your work experience in the field of medical imaging?

   In Years …….

c. Please fill in your highest degree (MSc/Ph.D.)

---

6. This question refers to the perceived usefulness and represents the perspective probability that a user increases the job performance and improves the quality of work.
   - ***Do you think that this dashboard can increase job performances for radiographers? Yes, or No - and explain your decision.***

7. The main interest is the perceived ease of use.
   - Is the color representation of the quality criteria (local contrast) ease to use?

8. The use of new technologies underlies external factors.
   - ***Which external variables can or may influence the acceptance for radiographers?***

   a.

   b.

   c.

   d.

9. Patient risk und misleading is a critical point for the quality toolkit.
   - ***Leads the visualization toolkit to a misleading interpretation or patient risk? Yes, or No and give some reasons***.

10. Some question about the dashboard.
    - ***Provides the dashboard all necessary information or is it overload in any way?***

E Comparison for the local and whole feature contrast table